# THE CONTRIBUTIONS OF SHEARWISE AND TRANSVERSE QUASI-GEOSTROPHIC VERTICAL MOTIONS TO BAROCLINIC CONVERSION

by

Nicholas R. Ofstun

A thesis submitted in partial fulfillment of the requirements for the degree

of

Master of Science

(Atmospheric and Oceanic Sciences)

at the

UNIVERSITY OF WISCONSIN-MADISON

2015

# ABSTRACT

The local energetics perspective of cyclogenesis focuses on quantifying the factors governing the tendency of eddy kinetic energy (EKE) associated with baroclinic disturbances. One of the largest components governing the evolution of EKE is the baroclinic conversion term, which represents the conversion between available potential energy and EKE. In the presence of a thermally-direct vertical circulation, the baroclinic conversion term is positive and thus serves as a source of EKE. The nature of thermally-direct circulations suggests that transverse quasi-geostrophic (QG) vertical motions would be largely responsible for the vertical motions associated with the baroclinic conversion process. However, previous work by Martin (2006) showed that shearwise QG vertical motions dominate the cyclogenesis process from the basic state variables perspective. Thus, it is possible that the energetics and basic state variable perspectives of cyclogenesis could be largely described by different species of vertical motions.

To investigate which species of QG vertical motion dominates the local energetics perspective of cyclogenesis through the baroclinic conversion process, a case study of two cyclones that developed nearly simultaneously over the North Pacific during October 2004 is considered. Two integration methods are used to track the contributions of shearwise and transverse QG vertical motions to the baroclinic conversion associated with each system: 1) A box-integration method that tracks the contributions within the geographic vicinity of each cyclone, and 2) A volume-integration method that tracks the contributions within EKE centers tied to the development of each cyclone. Using both methods, it is shown that shearwise vertical motions play a larger role in the baroclinic conversion process of each system than the transverse vertical motions.

Furthermore, differences in the energetics evolution of each cyclone are revealed. The first cyclone developed in association with positive baroclinic conversion, whereas the second cyclone's development was characterized by negative baroclinic conversion. Subsequent analysis reveals that the second cyclone received energy from upstream through ageostrophic geopotential fluxes dispersed by the first cyclone, following the "downstream development" paradigm postulated by Orlanski and Sheldon (1995). The potential implications of these results and further research questions are also discussed.

# ACKNOWLEDGEMENTS

First I would like to thank my advisor, Jon Martin, for providing me with guidance and invaluable suggestions while working on this thesis. This project has encompassed the better part of three years, spanning both my undergraduate and graduate school careers, and without Jon's help I would have never been able to complete it. I am honored to have worked with such a brilliant scientist and kindhearted person.

I would also like to thank the members of Jon's research group who have helped me along the way. Croix Christenson, Kyle Griffin, Zak Handlos, Melissa Breeden, and Andrew Winters have all offered advice and/or shared knowledge that has aided me in completing this thesis. I am extremely fortunate to have worked with such wonderful people and I know they will all do great things with their careers. I must also thank Pete Pokrandt, who was instrumental in providing the data and technical support needed to complete this project, as well as Michael Morgan and Matt Hitchman for providing constructive feedback that undoubtedly improved my thesis.

Finally, I need to thank my friends and family. All of their love and support has guided me my entire life, through the good times and the bad. As I complete my master's degree and take the next step in my career, know that I will be forever grateful for all that you have done for me.

# TABLE OF CONTENTS

# List of Figures

# Chapter 1: Introduction

## a. Energetics Background

The development of mid-latitude cyclones has been a central question in synoptic-dynamic meteorology for well over two centuries (Kutzbach 1979). Broadly speaking, there have been two major thrusts to such work since the middle of the last century. The older of these two perspectives, referred to as the basic state variables perspective by Martin (2006), involves examination of the interaction between identifiable upper tropospheric and lower tropospheric temperature and circulation disturbances. This perspective has been formalized in a variety of ways including the Sutcliffe (1947) development theorem and the various forms of the quasi-geostrophic omega equation (Petterssen 1956, Winn-Neilsen 1959, Trenberth 1978, and Hoskins et al 1978). Similar emphasis, minus any direct reference to vertical motion, also lies at the heart of the PV perspective of Hoskins et al (1985) and its accompanying diagnostic application by Davis and Emanuel (1991).

The newer perspective focuses on the energetics of growing baroclinic disturbances. Early studies by Robertson and Smith (1983) and Dare and Smith (1984) examined growing cyclones from an energetics approach using volume integrals over a broad domain spanning most of the continental United States and Canada. Later studies by Orlanski and Katzfey (1991), and Orlanski and Sheldon (1993) examined cases over smaller domains centered over the eastern Pacific Ocean in order to better quantify the tendency of eddy kinetic energy (EKE) associated with developing cyclones. This “local energetics perspective” of cyclogenesis focuses on quantifying the main factors contributing to the growth and/or decay of the EKE associated with baroclinic disturbances.

To perform this quantitative analysis, one needs to develop a time tendency equation for EKE. To derive this equation, the variables contained within the equations of motion must be partitioned into time-mean and eddy components. This partition is often performed using the notation:

$$X = X_m + x \tag{1.1}$$

where X denotes any vector or scalar quantity, subscript “m” references the mean part, and x refers to the eddy part. Using this approach, Orlanski and Sheldon (1995) define the time tendency equation of EKE in pressure coordinates as:

$$\frac{\partial K_e}{\partial t} = -(v \cdot \nabla \phi) - (\nabla \cdot (\boldsymbol{V} K_e)) - \frac{\partial(\omega K_e)}{\partial p} - \boldsymbol{v} \cdot (\boldsymbol{v} \cdot \nabla \boldsymbol{V}_m) + Residue \tag{1.2}$$

The term on the left hand side of (1.2) is the time tendency of EKE. The first term on the right hand side of (1.2) is the eddy advection of eddy geopotential height and represents work done by the pressure gradient force. This term can be further broken down into:

$$-\boldsymbol{v} \cdot \nabla \phi = -\nabla \cdot (\boldsymbol{v}\phi)_a - \omega\alpha - \frac{\partial(\omega\phi)}{\partial p} \tag{1.3}$$

The three terms on the right hand side of (1.3) represent three ways in which the EKE of a disturbance can be increased. The first term is the horizontal divergence of ageostrophic geopotential fluxes. The importance of ageostrophic geopotential fluxes in cyclone development was first postulated by Kung (1977). Defined for large-scale flows by Orlanski and Sheldon (1993) as:

$$(\boldsymbol{v}\phi)_a = \boldsymbol{v}\phi - \boldsymbol{k}\times\nabla\frac{\phi^2}{2f(y)} \tag{1.4}$$

this term represents the dispersion of EKE to another location, separate from the effects of advection. The third term on the right hand side of (1.3) is the vertical flux divergence of ageostrophic geopotential which redistributes energy vertically. Orlanski and Sheldon (1995) note that this term can be large locally, but is generally very small when integrated over the full depth of the atmosphere. As such, this thesis will not examine this term any further.

The second term on the RHS of (1.3) is the baroclinic conversion term, which represents the conversion of available potential energy into kinetic energy. The baroclinic conversion term is made up of ω, which, in this study, will represent the quasi-geostrophic vertical velocity, and α, which is directly related to the perturbation temperature of the atmosphere. From this, one can see that a thermally direct (indirect) circulation, with perturbation warm air rising (sinking) and/or perturbation cold air sinking (rising), will result in the baroclinic conversion term being positive (negative), creating (consuming) kinetic energy by lowering (raising) the center of mass of the fluid. Previous work has shown that strong ascent in the warm sector of a cyclone makes up a significant portion of the baroclinic conversion process (e.g. Orlanski and Katzfey 1991). Overall, a study by Orlanski and Sheldon (1993) argued that baroclinic conversion is the more dominant part of the energy budget in the lower troposphere, whereas horizontal ageostrophic geopotential flux tends to be the dominant energetics term in the upper troposphere.

Rewriting equation (1.2) with the expanded version of the eddy advection of eddy geopotential heights term produces the following:

$$\frac{\partial K_e}{\partial t} = -\nabla\cdot(\boldsymbol{v}\phi)_a - \omega\alpha - \frac{\partial(\omega\phi)}{\partial p} - (\nabla\cdot(\boldsymbol{V}K_e)) - \frac{\partial(\omega K_e)}{\partial p} - \boldsymbol{v}\cdot(\boldsymbol{v}\cdot\nabla\boldsymbol{V}_m) + R \tag{1.5}$$

The fourth, fifth, and sixth terms on the right hand side of equation (1.5) are the horizontal and vertical divergence of the EKE fluxes and the Reynolds stress, respectively. The Reynolds stress term represents a conversion from mean kinetic energy to EKE through the interactions between the time-mean and perturbation flows (Orlanski and Katzfey 1991, Lackmann et al. 1999). The last term includes all other terms not accounted for, including frictional dissipation and errors.

Lackmann et al. (1999) examined the mechanisms behind the intensification of an upper-tropospheric jet streak as part of an investigation into upper-tropospheric cyclogenetic precursors observed during the Experiment on Rapidly Intensifying Cyclones over the Atlantic second intensive observation period (ERICA IOP 2). Since jet streaks correspond to total kinetic energy maxima, examination of the local EKE budget provided physical insight into the development of this feature. Lackmann et al. found the Reynolds stress term to be the largest term of the EKE budget of a disturbance over North America. Noting that the Reynolds stress term is positive when the perturbation horizontal flow is orientated within 45 degrees of normal to the axis of dilatation of the time-mean flow, they concluded that the presence of a ridge over western North America favored the development of the jet streak over central North America. Specifically, the perturbation northwesterly flow east of the ridge axis provided a favorable orientation with respect to the time-mean flow for the contributions of the Reynolds stress term to be large.

Despite the prominence of the Reynolds stress term in the Lackmann et al. (1999) results, in most other reported cases the terms represented in (1.3) dominate the EKE budget, specifically the horizontal divergence of ageostrophic geopotential fluxes and baroclinic conversion terms (McLay and Martin 2002).

Therefore, recent work utilizing the local energetics perspective has focused primarily on the divergence of ageostrophic geopotential fluxes and baroclinic conversion terms, with the goal of quantifying the role of neighboring systems in the development of baroclinic disturbances. This idea, often characterized as “downstream baroclinic development” or “downstream development”, had been discussed in work as far back as Namias and Clapp (1944). However, Orlanski and Sheldon (1995) provided conceptual framework for the idea of downstream development in their three stage model of the energetic life cycle of baroclinic systems as shown in Fig. 1.1. In stage 1, a pre-existing energy center east of a trough begins to decay by dispersing EKE via ageostrophic geopotential fluxes. Due to the sub-geostrophic (super-geostrophic) flow and low (high) perturbation heights present in troughs (ridges), these fluxes are directed downstream to the east as the quantity $v'\phi'$ is positive. The convergence of ageostrophic geopotential fluxes on the eastern side of the downstream ridge contributes to the development of a new energy center (hereafter termed the western energy center). During stage 2, the western energy center continues to grow via the convergence of fluxes from the upstream center, but also begins to generate its own kinetic energy through baroclinic conversion. Because of the ageostrophic convergence and cold thermal profile typically found to the east of a ridge crest, a thermally direct circulation of cold air sinking is responsible for this baroclinic conversion. As the western energy center matures, it begins to disperse this energy downstream through its own fluxes. Convergence of these fluxes leads to the development of a new energy center (hereafter termed the eastern energy center) east of a subsequent trough axis. Ascent of warm air allows for the eastern energy center to further grow via baroclinic conversion. Lastly, during stage 3, the western energy center begins to dissipate from net ageostrophic geopotential flux divergence while the eastern energy center reaches maturity and begins to export energy even further downstream. As a result, the cycle potentially begins anew. In this way, an EKE center associated with a baroclinic disturbance will propagate downstream less quickly than the energy itself, resulting in the potential development of another system.

Numerous studies have attempted to document downstream development in real cases. Danielson et al. (2004) documented 41 cold-season cyclones that developed over the eastern North Pacific Ocean in an attempt to distinguish which cases were examples of downstream development. They tracked the evolution of three EKE centers across the Pacific (located over the western, central, and eastern Pacific, respectively) for each case. To classify a case as being an example of downstream development, they required that prior to the intensification of the eastern cyclone, there must be a period where an ageostrophic geopotential flux was directed from the western energy center towards the central energy center, and that a subsequent period of time existed when this flux was the dominant contributing factor to the growth of the central energy center. These same criteria were then applied to the development of the eastern energy center. Overall, they found that about half of their cases could be considered examples of downstream development, as kinetic energy generated through baroclinic conversion in upstream disturbances over the western North Pacific was dispersed downstream to aid in the development of the cyclones over the eastern North Pacific. A follow-up study employed a numerical simulation examining the effects of an upstream ridge and trough couplet on the subsequent downstream development of one of these cases (Danielson et al. 2006). To examine these effects, the authors changed the strength of the upstream ridge and trough couplet by modifying the eddy PV anomalies associated with each feature. They performed four different simulations, encompassing a control run (no eddy PV modification), a simulation where the eddy PV was fully removed from the trough and ridge, and half-removal and half-addition of the eddy PV amplitude simulations. The amount of baroclinic conversion occurring in the western cyclone and subsequent dispersion of EKE to the downstream, eastern cyclone was found to be directly correlated with the amplitude of the eddy PV features associated with the upstream ridge and trough couplet, thereby identifying the significance of these upstream features in the subsequent development of the cyclone over the eastern North Pacific.

An idealized modeling study by Schemm et al. (2013) comparing the formation of warm conveyor belts in dry and moist baroclinic waves also illustrated the downstream development paradigm. Their study showed that the primary cyclone that developed from the baroclinic wave was stronger in the moist simulation compared to the dry simulation, and the subsequent development of a downstream cyclone was observed to occur earlier in the moist simulation. Further analysis revealed that these differences could be largely attributed to the latent heating that occurred in the moist simulations. The latent heating in the moist simulation contributed to the development of a stronger upper-level negative PV anomaly compared to the dry simulation via the effects of diabatic PV redistribution. Subsequently, an enhanced downstream ridge was present in the moist simulation, leading to a stronger anticyclonic circulation at upper levels. This stronger circulation allowed for a greater southward directed flow downstream, contributing to the quicker development of a downstream trough and surface cyclone in the moist simulation. Moreover, the stronger negative PV anomaly in the moist simulation contributed to a larger PV-gradient downstream of the primary cyclone, corresponding to an enhanced wind-speed (and EKE) maxima. Examination of the energy budget revealed that the enhanced EKE maxima was primarily due to greater baroclinic conversion in the moist simulation as a result of condensational heating. As such, dispersion of energy downstream began earlier in the moist simulation, leading to the quicker development of a downstream cyclone. Moreover, a simulation employed by Papritz and Schemm (2013) examined the effects of a dry baroclinic wave on developing a primary cyclone and a subsequent downstream cyclone from the QG energetics perspective. They found that the downstream cyclone initially developed primarily due to the convergence of ageostrophic geopotential fluxes in the upper troposphere emitted from the kinetic energy center associated with the primary cyclone.

In the lower troposphere, baroclinic conversion also contributed to the development of the downstream kinetic energy center through the subsidence of cold air occurring from convergence downstream (upstream) of the ridge (trough) axis. At later times, as the downstream cyclone reached a more mature stage, baroclinic conversion from ascent in the warm sector in the lower troposphere became the primary source of kinetic energy. This energy generated by the downstream cyclone was in turn radiated away by ageostrophic geopotential fluxes, with fluxes directed downstream (upstream) in the upper (lower) troposphere. Fluxes that propagated upstream in the lower troposphere were consistent with the conceptual model of Orlanski and Sheldon (1995), who noted that upstream ageostrophic fluxes were possible at vertical levels where the mean flow was slower than the phase speed of the baroclinic wave. Thus, the concept of downstream development has been illustrated in idealized modeling studies of both dry and moist baroclinic waves, as well as in real case studies.

### b. Partitioning of Vertical Motion and Its Applications

Studying cyclogenesis *is aided by* an understanding of the vertical motions employed in the strengthening of a baroclinic disturbance. A cyclone cannot deepen without mass being evacuated from the atmospheric column as a result of divergent winds in the upper troposphere. In his pioneering study, Sutcliffe (1947) showed that the synoptic-scale vertical motion involved in cyclogenesis can be accurately diagnosed by considering vorticity advection by the thermal wind. The thermal wind relationship states that the geostrophic vertical shear is associated with horizontal gradients of temperature. As such, the thermal wind is aligned parallel to isentropes, meaning that vertical motions arising from vorticity advection by the thermal wind are distributed in couplets along the thermal wind (termed shearwise vertical motions by Martin (2006)). Later work by Sawyer (1956) and Eliassen (1962) demonstrated that frontal-scale vertical motions, organized in couplets that straddle the thermal wind, result from deformation of the lower tropospheric thermal field (frontogenesis). Specifically, when the magnitude of the horizontal temperature gradient is increased, a thermally direct circulation is forced that acts to relax this temperature gradient as warm (cold) air rising (sinking) cools (warms) adiabatically.

In relation to these two concepts, Keyser et al. (1992) examined the quasi-geostrophic (QG) vertical motions of an idealized model cyclone. Keyser et al. (1992) demonstrated that the total QG vertical motion was composed of two components, denoted $\omega_s$ and $\omega_n$, corresponding to the divergence of the along and across isentrope components of the ***Q***-vector. Following the geostrophic flow, these components of ***Q*** alter the direction and magnitude of the gradient of potential temperature, respectively.

Following this work, a pair of studies by Martin (1998a, 1998b) examined the structure and evolution of a continental winter cyclone, including an investigation into how cyclones developed an occluded structure. Defining the occluded structure as "1) the horizontal juxtaposition of two baroclinic zones separated by an axis of highest theta or theta-e, and 2) a sloping vertical axis of maximum theta-e extending from the surface to upper-tropospheric levels, that separates two regions of large horizontal theta-e gradient", Martin (1998a) found that the occluded structure developed first in the mid-troposphere and later near the surface.  Parcel trajectories employed in his study showed that the occluded structure developed as a result of the cold frontal zone encroaching upon and then ascending over the warm-frontal zone. This creates a three-dimensional sloping structure of warm air aloft, deemed the *trowal* by Penner (1955). In addition, Martin (1998b) showed that a significant portion of the so called “wrap around” precipitation that occurred to the northwest of the surface cyclone center originated from the ascent of warm, moist air through the trowal portion of the occluded structure as part of a “trowal airstream”. Subsequent analysis by Martin (1999) showed that the QG forcing for ascent in the trowal airstream of three cyclones was due largely to shearwise vertical motions as part of the convergence of the along-isentrope component of ***Q***. Moreover, it was shown that the same along-isentrope ***Q***-vector convergence was responsible for creating the characteristic thermal ridge present in the occluded structure as part of the rotational frontogenesis process. Thus, the partitioning of QG omega led to a broader understanding of extra-tropical cyclones by highlighting the dominant physical process behind the formation of the occluded structure.

With the realization that partitioning the QG vertical motion field could reveal deeper knowledge about synoptic dynamics, other studies utilized this technique to examine additional aspects of extra-tropical cyclones. For example, in a recent pair of papers (Martin 2006, 2007), the ***Q***-vector form of the QG omega equation (Hoskins et al. 1978) was employed to investigate some fundamental aspects of mid-latitude cyclogenesis. Particularly at issue was whether or not the separate transverse ($\omega_n$) and shearwise ($\omega_s$) QG omega fields, forced by the across- and along-isentrope components of ***Q***, respectively, play different roles in the life cycle of a mid-latitude cyclone. Based solely upon an examination of the distribution of these components of mid-tropospheric omega, Martin (2006) suggested that the updraft portions of the shearwise couplets (aligned *along* the thermal wind) were responsible for the origin and subsequent intensification of the lower tropospheric cyclone. The updraft portions of the transverse couplets (which *straddle* the thermal wind) were thought to make little contribution to the sea-level development until late in the cyclone life cycle. These suggestions were substantiated in the subsequent paper (Martin 2007) in which lower tropospheric height tendencies associated with each component of the QG omega were calculated and compared. It was found that the shearwise updrafts drive over 80% of the cyclogenetic height falls at least through the end of the mature stage of the life cycle. In the post-mature phase, any continued cyclogenesis was found to be driven nearly equally by the shearwise and transverse updrafts.

Partitioning of vertical motions has been used to examine other aspects of extra-tropical cyclones such as the development of upper level frontal systems. Characterized by enhanced baroclinicity and local maxima in wind speeds and vertical vorticity in the upper troposphere, upper level fronts have been shown to play an important role in cyclogenesis (eg. Lackmann et al. 1997). Pioneering work by Shapiro (1981) noted that upper fronts often form in flows characterized by temperature advection along a jet. Specifically, geostrophic cold air advection in the presence of cyclonic shear was found to be a favorable condition for forming upper fronts, as the subsidence branch of a thermally direct circulation was laterally displaced towards the warm side of a jet, resulting in subsidence beneath the jet core. Subsidence associated with this so-called “Shapiro effect” is largely responsible for the creation of the upper level frontal zone through the effects of tilting horizontally aligned isentropes into a more vertical orientation. Lang and Martin (2010) employed the partitioning of QG vertical motions to show that shearwise subsidence both contributes to the frontogenetical tilting effect that strengthens the horizontal temperature gradient at upper levels as well as provides a mechanism to initiate along flow cold air advection that can generate the Shapiro effect. Subsequent work by Lang and Martin (2012a, 2013b) examined how QG vertical motions were tied to the life cycle of upper tropospheric and lower stratospheric frontal systems. They found that geostrophic cold air advection in the lower stratosphere promoted QG subsidence on the cold side of the lower stratospheric front, which weakened due to the associated adiabatic subsidence warming. This subsidence extended into the upper troposphere such that it helped to strengthen the upper tropospheric frontal zone, which was already in a favorable environment for development characterized by cold air advection in cyclonic shear as part of northwesterly flow. The opposite occurred for cases of southwesterly flow, where geostrophic warm air advection promoted QG ascent that contributed to both the weakening of the upper tropospheric frontal zone and strengthening of the lower stratospheric frontal zone. Later work by Martin (2014) showed that the primary forcing for QG descent in cases of cold air advection in cyclonic shear was due to the advection of geostrophic shear vorticity by the thermal wind, which is a shearwise vertical motion. Moreover, it was shown that this mechanism for descent was just as (if not more) important than the “Shapiro effect” in contributing to the tilting frontogenesis of the developing upper front. Therefore, the partitioning of QG vertical motions has further advanced understanding of extra-tropical cyclones by dissecting the development of cyclogenetic features such as upper level frontal systems.

## c. Motivation

Examining aspects of extra-tropical cyclones through the partitioning of QG vertical motions has a recent but rich history that has led to a deeper understanding of the physical mechanisms that cyclogenesis. This work has complemented insights into cyclogenesis that have been obtained through use of the local energetics perspective. However, to the author's knowledge, these two techniques have never been combined in an attempt to deepen understanding of the processes governing the energetic evolution of mid-latitude cyclones. Referring back to (1.5), it is clear that terms involving fluxes serve as a means to redistribute, rather than create, EKE. Only the baroclinic conversion and Reynolds stress terms can generate or destroy EKE, though the Reynolds stress term tends to be much smaller outside of certain geographical locations (McLay and Martin 2002, Lackmann et al. 1999). Thus, baroclinic conversion is the primary means by which extra-tropical cyclones generate EKE, and non-zero baroclinic conversion only occurs in the presence of vertical motions and/or perturbation temperature distributions. As such, the baroclinic conversion term is an ideal candidate for further investigation using the partitioning of QG omega. Since $\omega_n$ is, by definition, a manifestation of either a thermally direct or thermally indirect circulation, one might expect that $\omega_n$ should dominate the baroclinic conversion in extra-tropical cyclones. Such a result would provide an interesting perspective to the process of cyclogenesis, as, in that case, the species of vertical motion that contributes most to energetic development would not be the species that contributes most to the development of the lower tropospheric circulation (Martin 2006, 2007). Moreover, the shearwise vertical motions that contribute significantly to the development of both upper fronts and the circulatory development of mid-latitude cyclones could potentially contribute little to the evolution of the EKE of these disturbances. This would imply the importance of differing physical processes when examining the development of extra-tropical cyclones from an energetics perspective.

This study will investigate this possibility by considering a case study of two cyclones that developed nearly simultaneously over the north Pacific Ocean during the early part of October 2004. First, a cyclone developed over the western North Pacific just off the coast of Japan ahead of an upper tropospheric wave. As this cyclone (hereafter referred to as the “western cyclone”) deepened, another system (hereafter referred to as the “eastern cyclone”) developed and underwent rapid intensification downstream over the eastern North Pacific, similar to the sequence that characterized a subset of the cases examined by Danielson et al. (2004). Analysis of the baroclinic conversion term associated with each cyclone reveals the relative contributions of the shearwise and transverse QG vertical motions to the overall energetics evolution of each system. The thesis is structured as follows. In Chapter 2, the data and methodology used to calculate the vertical motions and quantify the energetics evolution of each system is outlined. A synoptic overview of the two cyclones is presented in Chapter 3. In Chapter 4, the results of the energetics analysis are shown. Lastly, a summary and discussion of the results in the context of previous work examining the evolution of mid-latitude cyclones are presented in Chapter 5.

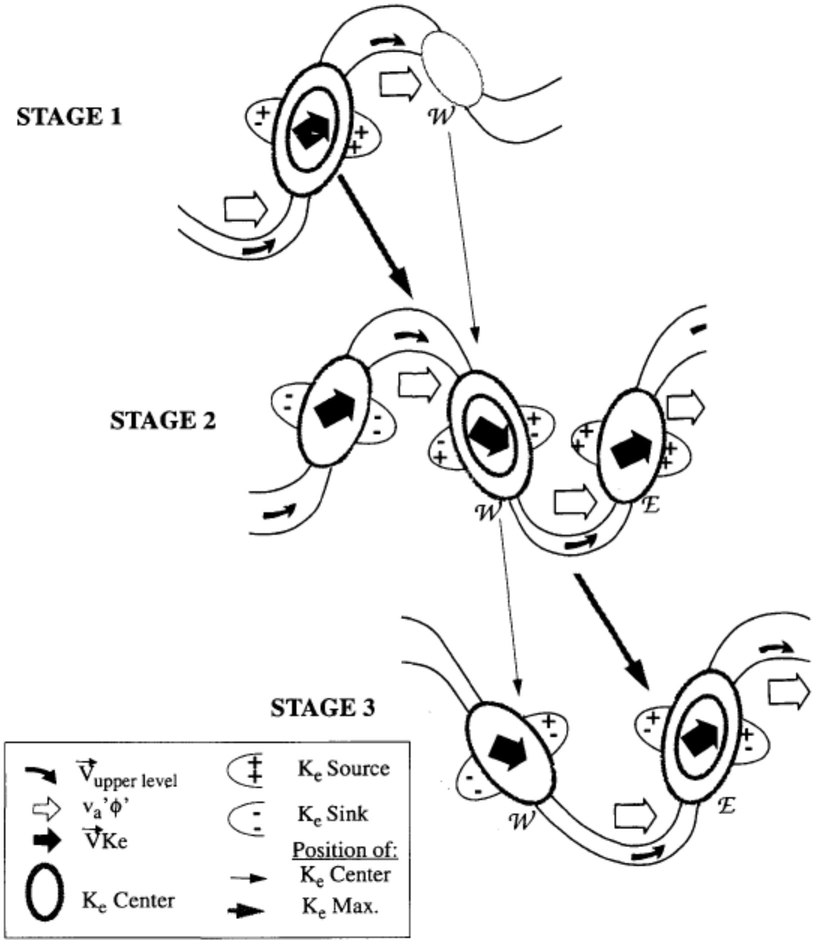

**Figure 1.1:** Figurative description of the downstream development paradigm, adapted from Orlanski and Sheldon (1995). Bold contours correspond to local EKE maxima as indicated within the legend. Thick arrows between stages track the movement of the maximum in EKE, while thin arrows track the movement of individual EKE centers. See text for a more thorough description of the physical processes occurring in each step.

# Chapter 2: Methodology

## a. Calculation of Primary Terms in the EKE Tendency Equation

The calculation of the baroclinic conversion term requires the use of both the perturbation specific volume, α, and the vertical velocity, ω. In this study, the contributions of partitioned vertical motions to the baroclinic conversion term is investigated. As such, calculations of the baroclinic conversion term are performed using the full QG vertical velocity as well as the partitioned components of the QG vertical velocity. From this point forward, the term “total baroclinic conversion” will refer to calculations of the baroclinic conversion term using the full QG vertical velocities, while the terms “shearwise baroclinic conversion” and “transverse baroclinic conversion” will refer to calculations incorporating the shearwise and transverse components of the QG vertical velocity, respectively. Calculations of the divergence of ageostrophic geopotential fluxes require the use of both perturbation winds and heights according to (1.4).

Calculations of all terms were performed in FORTRAN and GEMPAK at 50 hPa intervals from 950 hPa to 150 hPa, and then vertically averaged according to:

$$\acute{A} = \frac{1}{P_{top} - P_{bot}} \int_{P_{bot}}^{P_{top}} A$$

where A represents any variable, $P_{top}$ corresponds to 150 hPa, and $P_{bot}$ corresponds to 950 hPa. The integration was performed numerically using Simpson's rule. The following subsections describe how the perturbation temperatures, winds, and heights were calculated in order to obtain the perturbation specific volume and ageostrophic geopotential fluxes, and how the QG vertical velocity field was partitioned into the shearwise and transverse components.

### *i) Calculation of Perturbation Temperatures, Winds, and Heights*

To calculate the perturbation temperatures for each grid point in the domain, a 31 year average temperature was taken for each point at every 6 hours (00Z, 06Z, 12Z, 18Z) for October 6th and October 7th using the National Centers for Environmental Prediction's (NCEP) Climate Forecast System Reanalysis (CFSR) data for the years 1979-2009. Using these average temperatures, the perturbation temperatures were calculated by taking the observed temperature every 6 hours from 00Z 6 October 2004 to 18Z 7 October 2004 and subtracting the corresponding average temperature for that grid point. In this way, diurnal and seasonal effects were filtered out. The perturbation temperatures were then used to calculate the perturbation specific volume using the Ideal Gas Law:

$$\alpha = \frac{RT}{P}$$

where T is the perturbation temperature, R is the specific gas constant for dry air, and P is the pressure. The perturbation winds and heights were calculated from the same data set and in the same manner as the perturbation temperatures. These quantities were then used in calculating the magnitude of the divergence of ageostrophic geopotential fluxes.

### *ii) Partitioning of QG Omega*

To find the corresponding values of shearwise and transverse baroclinic conversion, the QG omega field was split into along and across isentrope components. Such an analysis was first undertaken by Keyser et al. (1992), who found that the total QG vertical motion could be decomposed into two parts corresponding to the divergence of the along and across isentropic components of the ***Q***-vector. A brief overview is given here with regards to how this partitioning of ***Q*** is performed but the reader is referred to Martin (2006) for a more thorough description.

The ***Q***-vector form of the Quasi-Geostrophic (QG) omega equation is

$$\left(\sigma\nabla^2+f_o^2\frac{\partial^2}{\partial p^2}\right)\omega=-2\nabla\cdot\boldsymbol{Q} \qquad (2.1)$$

where the ***Q*** vector is given by

$$\boldsymbol{Q}=-f_0\gamma\left[\left(\frac{\partial\boldsymbol{V}_g}{\partial x}\cdot\nabla\theta\right)\boldsymbol{i}+\left(\frac{\partial\boldsymbol{V}_g}{\partial y}\cdot\nabla\theta\right)\boldsymbol{j}\right] \qquad (2.2)$$

with $\gamma=(R/f_0p_0)(p_0/p)^{(cv/cp)}$, $\sigma$ is the static stability, and $f_0$ is the domain averaged value of the Coriolis parameter.

In the case of geostrophic and adiabatic flow, ***Q*** is equal to

$$\boldsymbol{Q}=f_0\gamma\frac{d}{dt_g}\nabla_p\theta \tag{2.3}$$

Thus, ***Q*** represents the Lagrangian time derivative of the gradient of potential temperature following the geostrophic wind. This means that the ***Q*** vector can alter both the magnitude and direction of $\nabla\theta$. The portion of the ***Q*** vector aligned across the isentropes ($\boldsymbol{Q_n}$) is that portion of ***Q*** in the direction of $\nabla\theta$ and is given by

$$\boldsymbol{Q}_n=\left(\frac{\boldsymbol{Q}\cdot\nabla\theta}{|\nabla\theta|}\right)\boldsymbol{n} \tag{2.4}$$

where **n** is the unit vector in the direction of $\nabla\theta$ given by

$$\boldsymbol{n}=\frac{\nabla\theta}{|\nabla\theta|} \tag{2.5}$$

Thus, $\boldsymbol{Q_n}$ can alter the magnitude, but not the direction, of $\nabla\theta$. The across isentrope component of QG omega can be found from $-2\nabla\cdot\boldsymbol{Q_n}$.

The along isentrope component of ***Q*** is that portion of ***Q*** directed along isentropes with cold air to the left. That direction is given by

$$\boldsymbol{s} = \boldsymbol{k} \times \boldsymbol{n} \tag{2.6}$$

so that $\boldsymbol{Q_s}$ becomes

$$\boldsymbol{Q}_s = \frac{\boldsymbol{Q} \cdot (\boldsymbol{k} \times \nabla\theta)}{|\nabla\theta|} \boldsymbol{s} \tag{2.7}$$

Thus, $\boldsymbol{Q_s}$ affects changes in the direction of ∇θ, but cannot affect its magnitude. The along isentrope component of QG omega is found from $-2\nabla \cdot \boldsymbol{Q_s}$.

The exact QG omega field is calculated using the numerical method of successive over relaxation (SOR) to solve for the f-plane version of the QG omega equation, with the geostrophic forcing calculated from the divergences of ***Q***, $\boldsymbol{Q_s}$, and $\boldsymbol{Q_n}$. In addition, it was assumed that there was not a mean background QG vertical velocity over the domain, such that derived values of omega in this study corresponded to perturbation values appropriate to use in the calculation of the baroclinic conversion term. The author justifies such an assumption by noting that the area encompassed by this case study is co-located with a synoptic storm track, so areas of upward and downward vertical motions should tend to average out over time.

## b. Description of Horizontal Integration Methods

In an attempt to track the relative contributions of the shearwise and transverse baroclinic conversion terms to the development of the two cyclones, energy budgets were calculated by horizontally integrating the vertically-averaged primary terms of the EKE tendency equation. This was done in two different ways as described in the following subsections.

### *i) The Box-Integrated Method*

The first method involved integrating the terms within quadrilaterals (or “boxes”) delineated by latitude lines on the northern and southern borders and longitude lines on the western and eastern borders. This was done in an attempt to document the evolution of the energetics in the direct geographic vicinity of the surface cyclones. The exact size and shape of the boxes, though admittedly arbitrary, attempted to capture the main pockets of baroclinic conversion located near the mean sea-level pressure minimum of each cyclone. While the location of the boxes associated with each storm varied at different times, the geographical area covered by the boxes remained approximately constant. The box around the western cyclone covered an area of about $4.70*10^6$ km$^2$, while the box around the eastern cyclone covered an area of about $3.96*10^6$ km$^2$. In addition, boxes were not constructed around the eastern cyclone until 12Z October 6th as this was the first time where there were signs of the developing storm at the surface as defined by sharp curvature in the 1012 hPa isobar. For reference, Fig. 2.1 shows the location and shape of each of the boxes at a sample time.

### *ii) The Volume-Integrated Method*

The second method performed the integration within volumes defined by EKE centers similar to the method employed by Danielson et al. (2004) (hereafter DGS). This was done both in order to document whether downstream development was a factor in the development of the eastern cyclone as defined by DGS, as well as to potentially support results from the box-integrated method in a less arbitrary manner from defining boxes around each system as the integrals are performed within EKE centers physically tied to the development of each system. The 175 $m^2/s^2$ contour of the vertically averaged EKE was used as the threshold for defining the EKE centers as this contour was small enough to incorporate the relevant features across the North Pacific basin while still large enough to filter out most of the background noise. For reference, Fig. 2.2 and Fig. 2.3 show the location of the different EKE centers at each time used in this study. As with DGS, there were three EKE centers of interest. A left EKE center was located in the western North Pacific and associated with the development of the western cyclone. A central EKE center was located downstream of the left EKE center and served as an intermediary between the western and eastern cyclones. After 00Z 7 October, a right EKE center associated with the development of the eastern cyclone split off from the central EKE center and was located over the eastern North Pacific. The labels L, C, and R shown on Fig 2.2 and Fig. 2.3 correspond to these left, central and right EKE centers respectively. At certain times it was hard to distinguish between the different EKE centers, so latitude and longitude lines were used to separate one EKE center from another. While also somewhat arbitrary, the choice of the dividing lines were made so that the left and right EKE centers remained spatially correlated with the western and eastern cyclones respectively, with the central EKE center in between. In addition, the calculations of each primary tendency term were normalized by dividing the volume-integrated terms by the whole volume-integrated EKE to express each term in terms of a growth rate. Such a normalization allows for the comparison of terms that may potentially differ by several orders of magnitude.

Thus, the use of the volume-integrated method allows for the calculation of the primary tendency terms within the EKE centers that were physically tied to the development of each cyclone. In contrast, the box-integrated method performs the calculation of each term within the geographic vicinity of each cyclone. Comparison between the results of each method allows for support of the otherwise arbitrary choices in the bounding contours delineating the boxes and EKE centers. All calculations for both the volume and box integrated methods were performed using MATLAB scientific programming software.

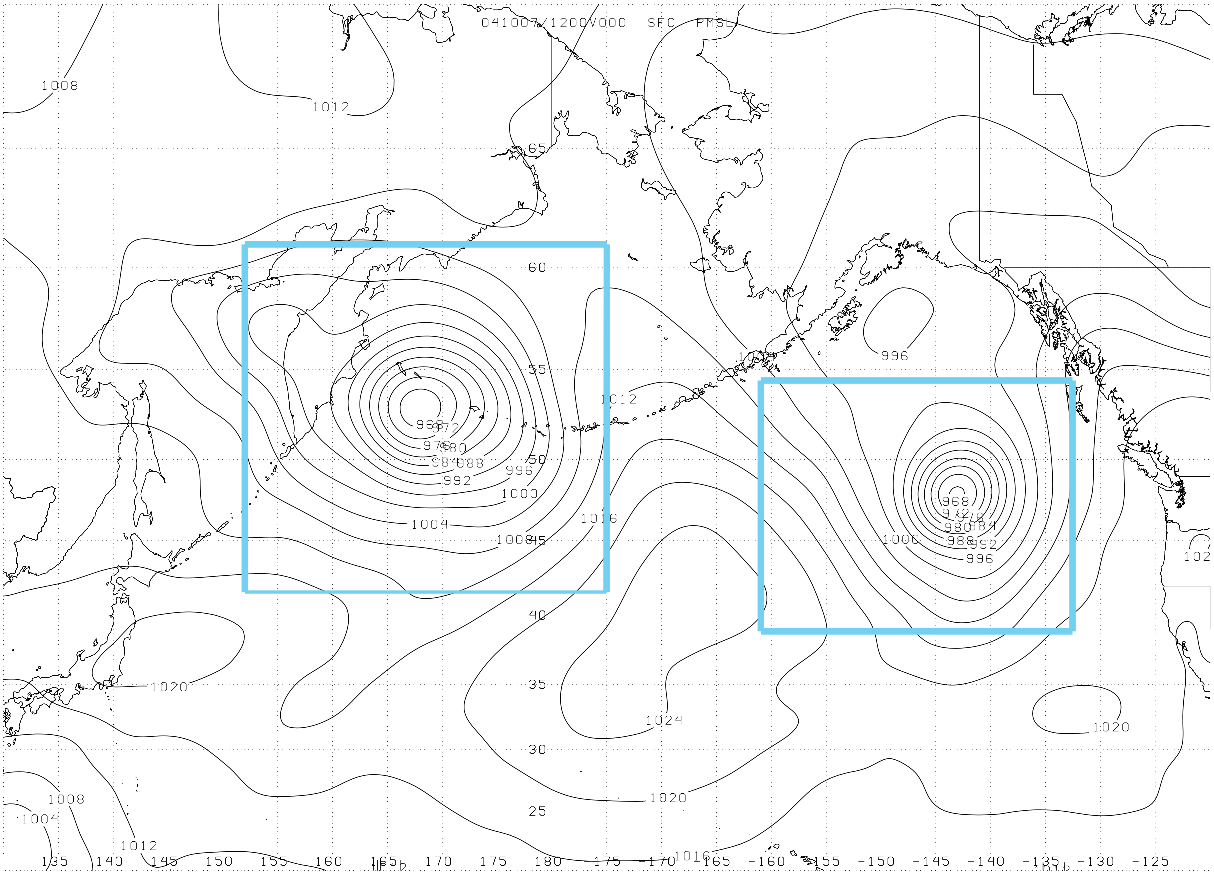

**Figure 2.1:** Illustration of the boxes used for integrating the vertically-averaged primary terms of the EKE tendency equation associated with the western and eastern cyclones on 12Z October 7th. Light blue lines delineate the boundaries of each box. Mean sea-level pressure (solid black), contoured every 4 hPa, is shown along with parallels and meridians (gray dash) for reference.

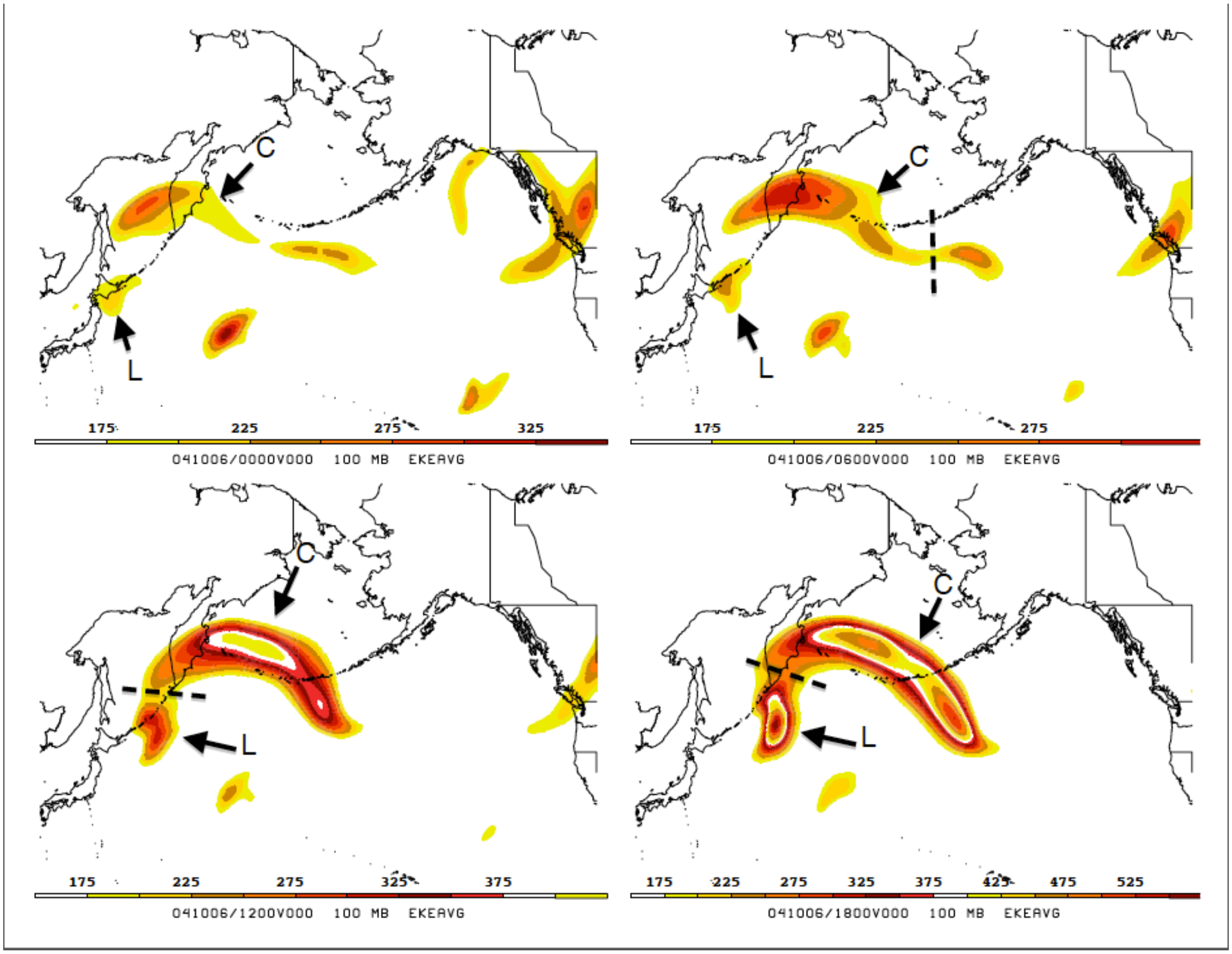

**Figure 2.2:** Vertically averaged EKE (fill) contoured every 25 m$^2$/s$^2$ beginning with 175 m$^2$/s$^2$ on 00Z (upper-left), 06Z (upper-right), 12Z (bottom-left), and 18Z (bottom-right) 6 October. Black arrows labeled “L”, “C”, and “R” denote the left, central, and right EKE centers at each time. Dashed black lines indicate approximate location of delineating boundary between two EKE centers.

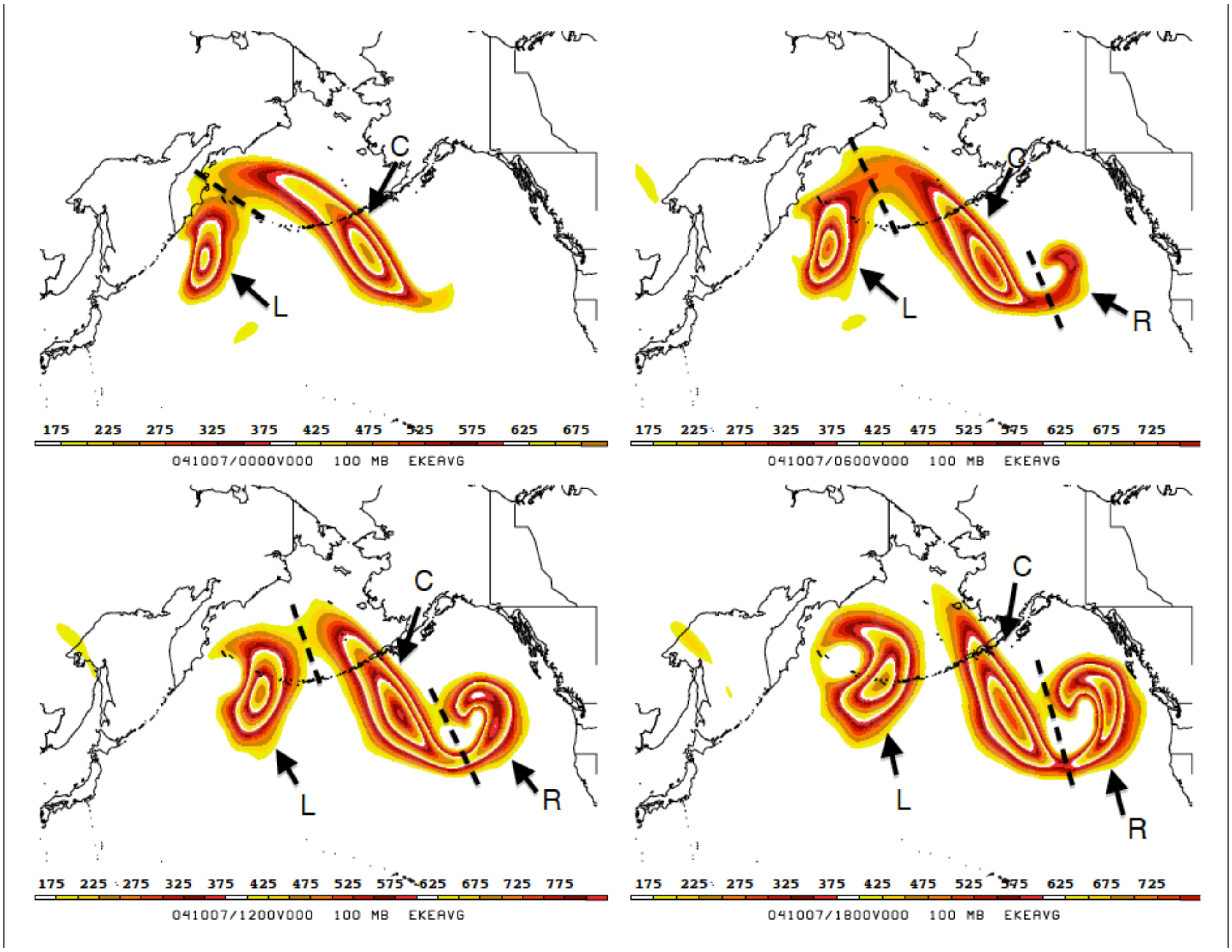

**Figure 2.3:** As with Fig. 2.2, except showing times on 7 October corresponding to 00Z (upper-left), 06Z (upper-right), 12Z (bottom-left), and 18Z (bottom-right).

# Chapter 3: Synoptic Overview

In this chapter a brief overview of the development of the two object cyclones over the North Pacific is presented. Though the data for this study covers the period from 00Z 6 October to 18Z 7 October, only three times separated by 18 hours are shown here for the purpose of brevity. These times capture the relevant features associated with the development of each system. Analysis from multiple pressure levels will be presented at each time to highlight important synoptic features tied to each cyclone's development, beginning with 00Z 6 October.

## a. 00Z 6 October

Figure 3.1 reveals the synoptic environment at four different pressure levels on 00Z 6 October. At this time, there was a slightly negatively tilted trough present at 300 hPa centered just off the northwest coast of Japan which was tied to the development of the western cyclone (Fig. 3.1a). Rounding the base of this trough was a jet streak with maximum wind speeds in excess of 55 $ms^{-1}$. Slightly downstream of this feature, there was a low-amplitude ridge extending northward from the west-central Pacific to the Kamchatka Peninsula. Extending from the ridge crest across the North Pacific was a more zonally orientated jet streak. Within this jet streak the most prominent of speed maxima- a region of winds in excess of 70 $ms^{-1}$- was located just south of the Aleutian Island chain. Over the Gulf of Alaska, there was a cutoff low in the geopotential height field tied to a decaying surface cyclone that was separate from the two systems investigated in this thesis. Such decaying features are common over this location during Northern Hemisphere fall and winter (Martin et al. 2001).

At 500 hPa, the shortwave trough over Japan was more positively tilted (Fig. 3.1b). A region of mid-tropospheric baroclinicity was co-located with this trough. Another region of modest baroclinicity was present near the western end of the Aleutians downstream of the ridge axis off the coast of the Kamchatka Peninsula. There was a small hint of a developing shortwave over this region that would contribute to the eastern cyclone's development at later times. Sharper curvature in the flow was present just off the eastern coast of Japan at 700 hPa, nearly forming a cutoff geopotential minimum in association with the developing western cyclone (Fig. 3.1c). This curvature was co-located with a region of perturbation warm air, characterized by warm anomalies as large as 6 K slightly to the east. The choice to show perturbation temperatures at 700 hPa was made to coincide with a level where vertical motions are typically strong since temperature anomalies and vertical motion are directly related to the calculation of the baroclinic conversion term. Over the central North Pacific, the small amplitude shortwave just south of the Aleutian Islands that was tied to the developing eastern cyclone straddled cold and warm temperature anomalies to the north and south, respectively.

At the surface, the developing western cyclone had a minimum in mean sea-level pressure (MSLP) of 1004 hPa (Fig. 3.1d). This surface low was located off the coast of Japan, consistent with the westward tilting vertical structure characteristic of developing baroclinic systems. There were signs of a developing cold-frontal zone extending to the southwest of this MSLP minimum, with a more weakly defined warm frontal zone to the north and east. Beneath the ridge at upper levels there was a high pressure system located over the central North Pacific. Slightly downstream of this surface high there was a small pressure trough co-located with a broad region of lower-tropospheric baroclinicity. This trough represented the initial manifestation of the eastern cyclone at the surface, which was still too weak to show a cutoff pressure contour at this time. Over the Gulf of Alaska the surface low associated with the upper level cutoff feature had a MSLP minimum of 976 hPa.

### b. 18Z 6 October

By 18Z 6 October, the shortwave trough associated with the western cyclone had become more negatively tilted at 300 hPa as it migrated northeastward over the western North Pacific (Fig. 3.2a). A jet streak with winds now in excess of 60 $ms^{-1}$ was still present at this time, with the left exit region of the jet in a favorable position to further aid in the development of the surface cyclone. Further downstream, the ridge spanning the central North Pacific had become slightly more amplified perhaps in response to downstream ridge-building associated with the western cyclone. As such, the shortwave trough associated with the eastern cyclone had become more amplified during this time as well. The jet streak over the central North Pacific had propagated slightly downstream of the ridge axis, with the maximum wind speeds now in excess of 75 $ms^{-1}$.

At 500 hPa, the shortwave trough associated with the western cyclone now had a mostly neutral tilt, although the curvature at the base of the trough had intensified in comparison to 18 hours earlier (Fig. 3.2b). There were signs of a developing thermal ridge at this level just to the east of this trough axis in association with the baroclinicity present over the region. The shortwave trough associated with the development of the eastern cyclone was clearly distinguishable downstream of the ridge axis over the central North Pacific. A thermal trough co-located with this shortwave hinted at the organizing frontal structure tied to the eastern cyclone developing in the lower troposphere. At 700 hPa, cold anomalies in excess of 7 K were co-located with the eastern cyclone shortwave, which was much easier to distinguish at this pressure level (Fig. 3.2c). To the south of the trough axis there were still slightly positive temperature anomalies. Further upstream, the warm anomalies associated with the western cyclone cutoff in geopotential grew even larger in magnitude, with values now in excess of 10 K.

By this time, the MSLP minimum of the western cyclone had dropped to 988 hPa in response to the favorable dynamics at upper levels (Fig. 3.2d). Clear evidence of both cold frontal and warm frontal structures were present to the south and east, respectively. Further to the east, there was now a more notable pressure trough in association with the eastern cyclone, with minimum pressures below 1008 hPa. The low-level baroclinicity in this area also indicated signs of developing frontal zones extending to the southwest and southeast from the base of the pressure trough. Further to the northeast, the decaying system over the Gulf of Alaska continued to weaken as the MSLP minimum rose from 18 hours earlier.

### c. 12Z 7 October

By 12Z 7 October, the trough at 300 hPa associated with the western cyclone had elongated and now extended from the Sea of Okhotsk to the tip of the Aleutian Island chain (Fig. 3.3a). Within this trough, a cutoff low developed as the western cyclone strengthened. In addition, the ridge downstream of this system continued to amplify, while a 55 ms$^{-1}$ jet streak remained in a favorable position to continue the growth of the western cyclone. South of the Gulf of Alaska, the trough associated with the eastern cyclone exhibited more curvature. By now the jet streak that had originally been characterized by mostly zonal flow on 00Z October 6th had developed a much more meridonal flow pattern, with northwesterly (southwesterly) flow upstream (downstream) of the curvature maxima. The maximum wind speeds in this jet streak were now in excess of 80 ms$^{-1}$.

At 500 hPa, cutoff lows in the geopotential height field were present with both the western and eastern cyclones, signaling that both of these systems were reaching a mature stage (Fig. 3.3b). In addition, thermal ridges were nearly co-located with both of these cutoff lows. However, the 700 hPa perturbation temperatures in the vicinity of each system remained quite different (Fig. 3.3c). Warm anomalies near 10 K continued to characterize the environment around the western cyclone in sharp contrast to the environment associated with the eastern cyclone, which was largely surrounded by cold temperature anomalies. The dividing line between the main warm and cold temperature perturbations was nearly coincident with the upstream ridge axis, as warm (cold) anomalies existed mostly in the southwesterly (northwesterly) flow upstream (downstream) of the ridge crest.

The MSLP minimum for both the western and eastern cyclones had dropped to 968 hPa by this time (Fig. 3.3d). The western cyclone was beginning to show signs of occlusion, as the storm center was nearly cutoff from the peak of the warm sector. In addition, the northern edge of the cold frontal zone nearly coincided with the eastern edge of the warm frontal zone. The warm front of the western cyclone nearly extended all the way to the southeast to join with the cold front of the eastern cyclone, separated only by a region of weaker baroclinicity beneath the surface high over the central North Pacific. A warm front was harder to discern in association with the eastern cyclone, though the system was firmly entrenched in the peak of the thermal ridge.

### d. Summary

The development of these companion systems proceeded in a manner similar to other sequential explosive cyclogenesis events documented over the North Pacific (eg., Sanders and Gyakum, 1980; Roebber, 1984; DGS) with a rapidly developing surface cyclone over the eastern North Pacific developing downstream of a predecessor rapidly developing feature over the western North Pacific. Both the western and eastern cyclone fall under the “bomb” definition employed by Sanders and Gyakum (1980). As shown in Fig. 3.4, the western cyclone experienced an extended period of development (42 h, from 00Z 6 October to 18Z 7 October) wherein the MSLP minimum dropped by 45 hPa from 1003 hPa to 958 hPa. A more rapid, but less prolonged period of development characterized the eastern cyclone where the minimum dropped 44 hPa from 1009 hPa to 965 hPa in the 30 hour period from 12Z 6 October to 18Z 7 October.

Overall, the developments of these two systems were fairly similar to each other. In both cases, an upper level trough encroached upon a region of baroclinicity, which led to the development of a cyclone at the surface. In addition, both systems had notable jet streaks in favorable positions to aid in their development. The main notable difference between the two developments were the perturbation temperatures in their respective surrounding environments. The western cyclone environment was dominated by warm temperature anomalies, whereas the eastern cyclone environment was dominated by cold temperature anomalies. The impact of these differing perturbation anomalies on the energetic evolution of the two systems will be described in the next chapter.

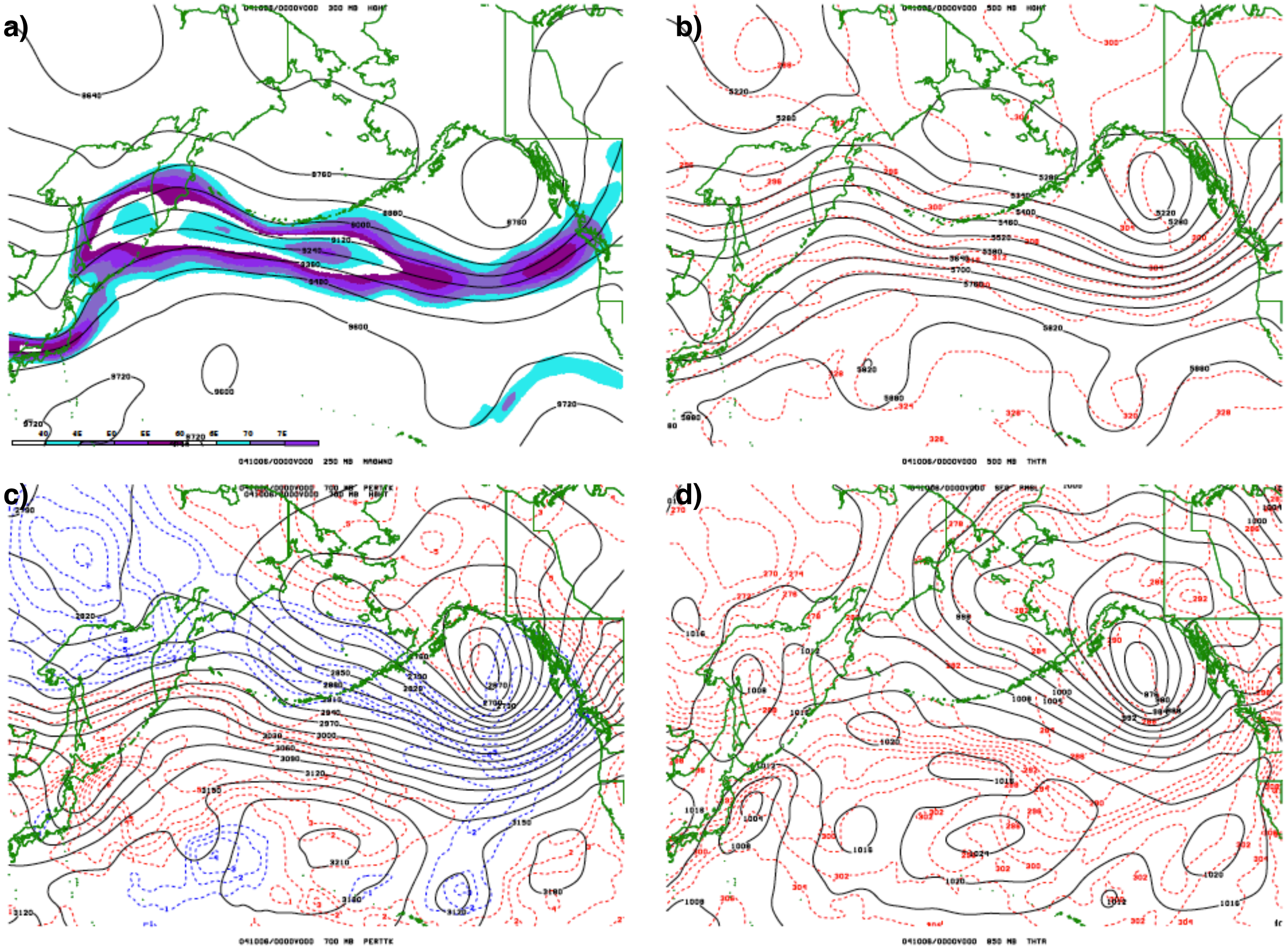

**Figure 3.1: a)** 250 hPa wind speeds (fill), contoured every 5 ms$^{-1}$ beginning at 40 ms$^{-1}$, and 300 hPa geopotential heights (solid black) contoured every 120 m, on 00Z 6 October. **b)** 500 hPa potential temperatures (dashed red) contoured every 4 K, and 500 hPa geopotential heights (solid black) contoured every 60 m, on 6 00Z October. **c)** 700 hPa warm (dashed red) and cold (dashed blue) temperature anomalies contoured every 1 K, and 700 hPa geopotential heights (solid black), contoured every 30 m, on 00Z 6 October. **d)** 850 hPa potential temperatures (dashed red) contoured every 2 K, and mean sea-level pressure (solid black) contoured every 4 hPa, on 00Z 6 October.

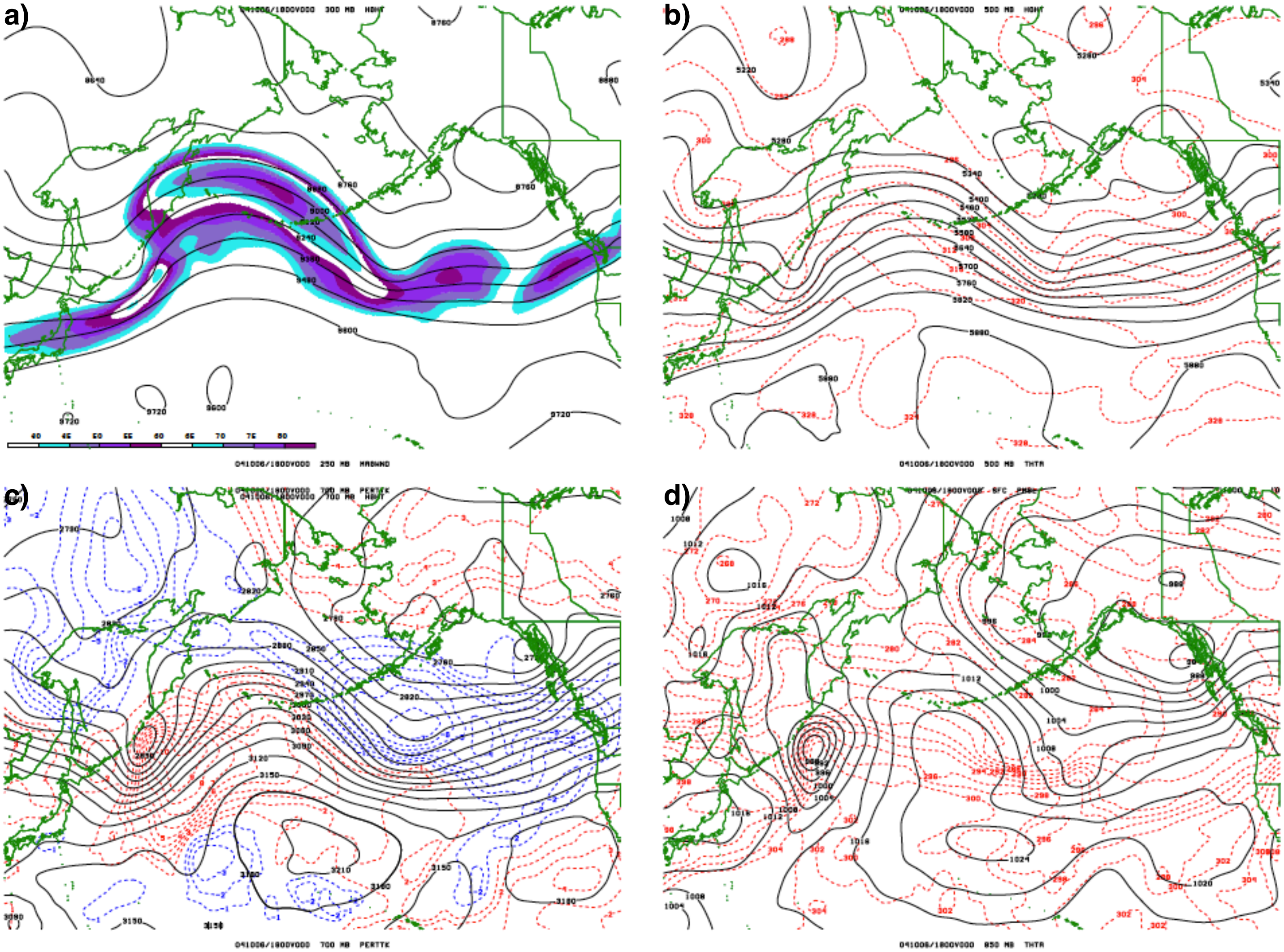

**Figure 3.2: a)** As for Fig. 3.1a, except on 18Z 6 October. **b)** As for Fig. 3.1b, except on 18Z 6 October. **c)** As for Fig. 3.1c, except on 18Z 6 October. **d)** As for Fig. 3.1d, except on 18Z 6 October.

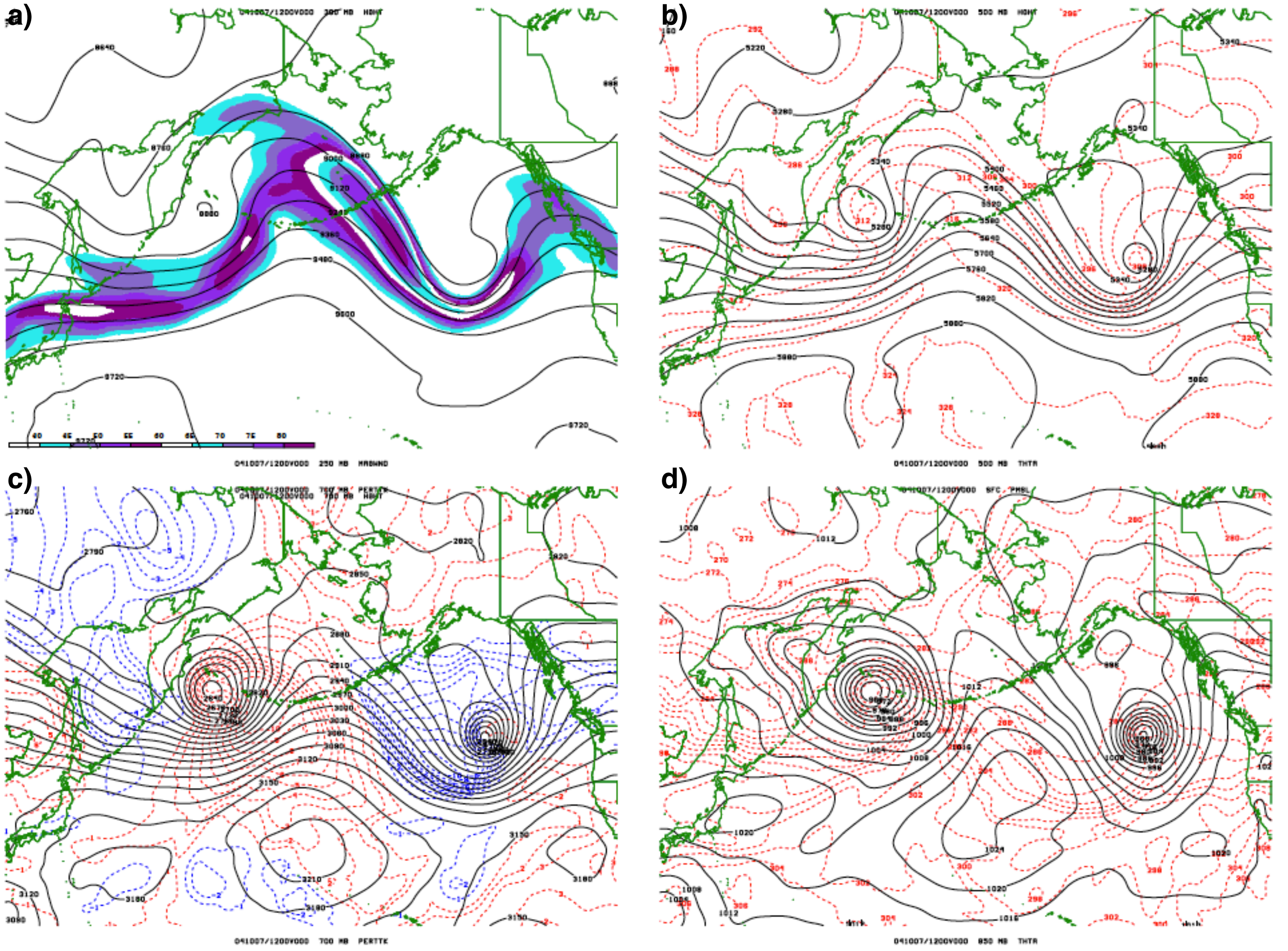

**Figure 3.3: a)** As for Fig. 3.1a, except on 12Z 7 October. **b)** As for Fig. 3.1b, except on 12Z 7 October. **c)** As for Fig. 3.1c, except on 12Z 7 October. **d)** As for Fig. 3.1d, except on 12Z 7 October.

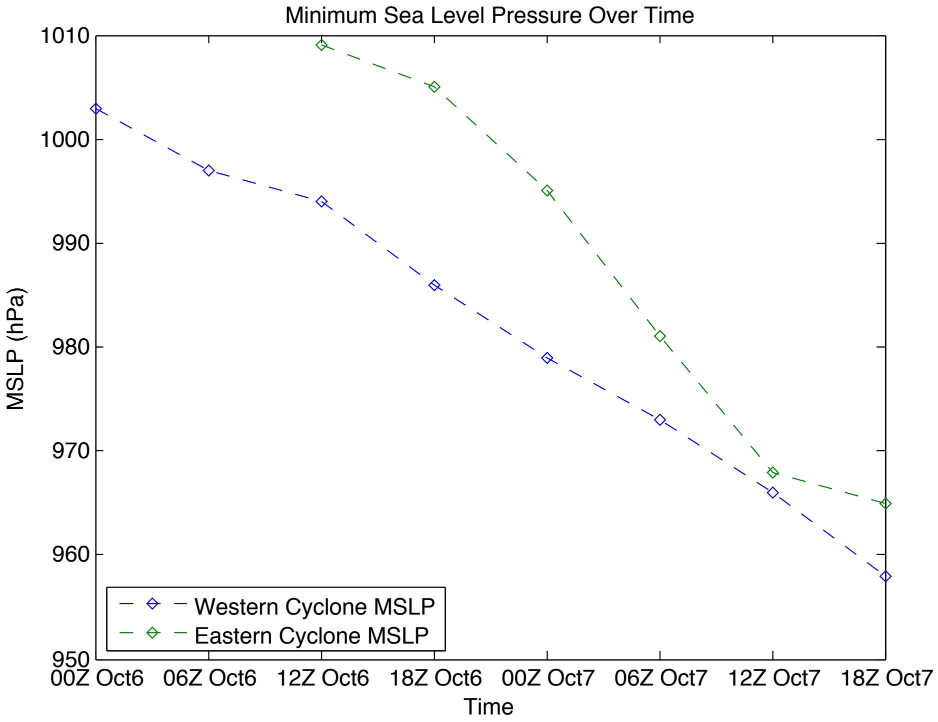

**Figure 3.4:** Minimum Sea Level Pressure in hPa plotted as a function of analysis time for the western (blue dash) and eastern (red dash) cyclones.

# Chapter 4: Energetics Analysis

In this chapter, the energetics evolution of the two cyclones described in Chapter 3 will be presented, focusing on the two largest terms in the EKE tendency equation (i.e., the baroclinic convergence term and the divergence of ageostrophic geopotential fluxes), with emphasis on the partitioned components of the baroclinic conversion term. First, a broad overview will be given of the evolution of the baroclinic conversion term at the same times highlighted in the previous chapter. Next, the evolution of the EKE budget focusing on the two primary terms of the EKE tendency equation will be discussed in association with each cyclone. This will be presented in two ways, using both the box-integrated and volume-integrated methods described in the methodology section. The use of the volume-integrated method allows for a classification of downstream development similar to that presented in DGS. Lastly, vertical cross-sections of baroclinic conversion will be examined in an attempt to provide context for the results revealed by the horizontal integration methods.

## a. Geographical Overview of Total and Partitioned Baroclinic Conversion

### *i) 00Z 6 October*

On 00Z 6 October, there was a small amount of positive baroclinic conversion occurring mainly to the north and east of the MSLP minimum associated with the western cyclone (Fig. 4.1a). Given the presence of warm perturbation temperatures in this area (refer to Fig. 3.1c), this baroclinic conversion was associated with ascending air tied to the developing system at the surface. Slightly further downstream, there were isolated pockets of both positive and negative baroclinic conversion occurring in association with the surface high near the western end of the Aleutian Island chain. Knowing that 700 hPa warm (cold) anomalies were present in this area associated with the negative (positive) baroclinic conversion, one can surmise that subsidence near the surface high was responsible for the baroclinic conversion as part of a thermally indirect (direct) circulation. There were other small pockets of positive and negative baroclinic conversion in the vicinity of the decaying system over the Gulf of Alaska, but there was little sign of any other significant baroclinic conversion across the eastern Pacific, particularly in what would become the development region of the eastern cyclone.

Partitioning the vertical motion field into shearwise and transverse components reveals that shearwise baroclinic conversion made up the majority of the total baroclinic conversion in the vicinity of the western cyclone at this time (Fig. 4.1b). Interestingly, the shearwise baroclinic conversion was spatially limited to the part of the total baroclinic conversion that extended north of the western cyclone. The transverse baroclinic conversion was less prominent in this region, and was instead confined to the area of total baroclinic conversion extending to the east of the western cyclone along the location of the developing surface warm front (Fig. 4.1c). The shearwise baroclinic conversion was also just as large (if not larger) than the transverse baroclinic conversion associated with the pockets of baroclinic conversion occurring near the surface high downstream and the decaying system over the Gulf of Alaska.

### *ii) 1800Z 6 October*

By 18Z 6 October, the total baroclinic conversion near the western cyclone center had increased substantially from 18 hours earlier (Fig. 4.2a). A small pocket of negative baroclinic conversion was located back to the southwest. Given the warm temperature anomalies still present over this area (refer to Fig. 3.2c), this corresponded to a region of subsidence present in the wake of the cyclone center. This subsidence was the downward vertical motion portion of a strong dipole of vertical motion associated with the development of the system. Over the eastern Pacific, there were two notable features in association with the developing eastern cyclone. Just upstream of the eastern cyclone, there was a pocket of positive baroclinic conversion resulting from subsiding cold air as inferred from the perturbation temperature distribution at that time. However, co-located with the developing pressure trough was a region of negative baroclinic conversion associated with the ascent of perturbation cold air. Thus, at this time, the development of the eastern cyclone was characterized by a distribution of baroclinic conversion actually opposite to that associated with a canonical development scenario.

The shearwise baroclinic conversion continued to make up the majority of the total baroclinic conversion occurring near both the western and eastern cyclones (Fig. 4.2b). This was especially true for both the positive baroclinic conversion center slightly upstream of the eastern cyclone and the negative baroclinic conversion center co-located with the developing pressure trough of the eastern cyclone. Moreover, the spatial pattern of the shearwise baroclinic conversion was almost identical to that of the total baroclinic conversion for these two areas. For the positive center near the western cyclone, the shearwise baroclinic conversion did not extend quite as far eastward as the total baroclinic conversion. This eastward extension area was associated with the transverse component of the baroclinic conversion, which also extended both further eastward and southward than the total baroclinic conversion center near the western cyclone (Fig. 4.3c). This was consistent with the presence of well developed frontal zones (refer to Fig. 3.2d) characterized by transverse bands of vertical motion as part of a thermally direct circulation.

### *iii) 1200Z 7 October*

At 12Z 7 October, the negative baroclinic conversion center associated with the eastern cyclone had strengthened and was still present in the northwestern portion of the storm, which had continued its rapid development in spite of the unusual location of this EKE sink (Fig. 4.3a). On the southern edge of the eastern cyclone, there was now a positive baroclinic conversion center that was connected to the dominant positive baroclinic conversion feature just upstream. This center likely played a role as a source of EKE for the eastern cyclone as will be described in the next section. Upstream, the positive baroclinic conversion near the western cyclone center had further strengthened over the preceding 18 hours in accordance with the development of the surface cyclone. Interestingly, the shape of this positive center resembled the classical comma-head cloud structure associated with mid-latitude cyclones. This was likely a manifestation of the distribution of vertical motions along the cold and warm fronts as well as near the cyclone center.

Both the shearwise (Fig. 4.3b) and transverse (Fig. 4.3c) baroclinic conversion components in each storm increased in accordance with the total baroclinic conversion. As at prior times, however, the shearwise component maintained its dominance over the transverse component. Of note, however, is that the transverse component nearly equaled the shearwise component in the positive baroclinic conversion center just upstream of the eastern cyclone. The positive centers in the southern region of the eastern cyclone and the northeastern region of the western cyclone were still dominated by the shearwise baroclinic conversion component. The transverse baroclinic conversion component still appeared most prominent in the vicinity of the cold and warm fronts of the western cyclone at this time (refer to Fig. 3.3d).

## b. EKE Budget Analysis

### *i) Box-Integrated Budgets of Western and Eastern Cyclones*

Before delving into the individual terms that contributed to the tendency of the EKE associated with each system, it is prudent to examine the total, box-integrated EKE of each storm. The EKE associated with the eastern cyclone during the two analysis times preceding the development of the surface cyclone was calculated using the same box as that used for 12Z 6 October. This was done in order to investigate the tendency of EKE just prior to the development of the eastern cyclone. Throughout the time period under consideration, the EKE of the western cyclone grew in magnitude (Fig. 4.4). This was true for the eastern cyclone as well, with the exception of the period from 12Z 6

October to 18Z 6 October. After this time, the rate of growth of EKE associated with the eastern cyclone was greater than that of the western cyclone, resulting in the EKE of the eastern cyclone becoming larger in magnitude after 06Z 7 October. The primary terms of the EKE tendency equation associated with each cyclone will now be discussed.

Figure 4.5a shows the box-integrated baroclinic conversion term (total and partitioned components) at each time for the western cyclone. Throughout the time period studied, the total baroclinic conversion remained positive near the western cyclone, thus providing a net source of EKE during the system's development. Moreover, the total baroclinic conversion was progressively stronger at each time until 12Z 7 October, after which it began to decay. During the time that the total baroclinic conversion was increasing, the shearwise baroclinic conversion was comparable to the transverse baroclinic conversion and was, in fact, larger at every time except on 00Z 7 October. Interestingly enough, the shift from shearwise dominance to transverse dominance that occurred between 18Z 6 October and 00Z 7 October also corresponded to the slowest rate of growth for the total baroclinic conversion. The same shift from shearwise to transverse dominance occurred during the lone declining phase of the total baroclinic conversion at the end of the analysis time as well.

The magnitude of the ageostrophic geopotential flux term (both divergence and convergence) for the western cyclone is shown in Fig. 4.5b. At all times, the divergence of fluxes is greater than the convergence, resulting in the net ageostrophic geopotential flux term being positive. This means that throughout the time period studied, the western cyclone was exporting more energy out of the box than it was receiving, resulting in a net sink of EKE. Moreover, the amount of ageostrophic geopotential flux divergence was greater than the total baroclinic conversion in the vicinity of the western cyclone at all times (Fig. 4.5c). However, because of the contributions of ageostrophic geopotential flux convergence, the net loss of EKE from ageostrophic geopotential flux divergence was more than offset by the total baroclinic conversion. As a result, the EKE of the western cyclone was able to grow throughout the analysis period.

The evolution of the baroclinic conversion term was much different for the eastern cyclone (Fig. 4.6a). Until 00Z 7 October, the total baroclinic conversion in the vicinity of the eastern cyclone was negative, effectively acting as a sink of EKE. After this time, the total baroclinic conversion transitioned to being positive and grew in magnitude over time, though it never became quite as strong as that associated with the western cyclone. The negative total baroclinic conversion before 00Z 7 October was largely a result of the negative shearwise component. Although the shearwise component grew more positive throughout the analysis time period, it did not become positive until after 06Z 7 October. In contrast, the transverse component remained positive throughout the analyzed time period, and grew successively larger between each time step after 18Z 6 October. As such, the transverse component compensated for the negative shearwise component in order to produce net positive total baroclinic conversion between 00Z and 12Z 7 October. Interestingly enough, this time period coincided with the largest 12 hour drop in MSLP of the eastern cyclone (refer back to Fig. 3.4).

Figure 4.6b reveals that the ageostrophic geopotential flux term was also a net sink of EKE throughout the analysis period for the eastern cyclone. There were a few time periods where the magnitude of ageostrophic geopotential flux convergence was comparable to that of the ageostrophic geopotential flux divergence, but never greater. After 00Z 7 October, the positive contributions of the baroclinic conversion term were able to overcome the net ageostrophic geopotential flux divergence to help facilitate a net growth of EKE (Fig. 4.6c). Before this time, however, the primary terms of the EKE tendency equation suggested that the rapid development of the eastern cyclone was associated with a net loss of EKE.

Thus, the eastern cyclone was able to grow in spite of the baroclinic conversion and ageostrophic geopotential flux terms acting as net sinks of EKE before 06Z 7 October. Nevertheless, the box-integrated EKE associated with the eastern cyclone was able to grow or nearly maintain itself during this time period (refer back to Fig. 4.4). A simple comparison between the starting and ending values of EKE associated with the eastern cyclone shows that the eastern cyclone gained .75 $m^2/s^3$ over the course of the analysis time period. However, when calculating how the EKE budget should have changed based solely on the baroclinic conversion and ageostrophic geopotential flux terms, the eastern cyclone should have experienced a net loss of about 1.06 $m^2/s^3$ during this same time period. While other terms in the EKE tendency equation may have been contributing to the growth of the eastern cyclone to account for this apparent discrepancy, the author postulates that the calculation of the ageostrophic geopotential flux term is sensitive to the integration method used. That is, the wide geographical area covered by the box may capture regions further from the eastern cyclone center with net ageostrophic geopotential flux divergence, resulting in contributions from any flux convergence near the cyclone center being mitigated when integration is performed. A similar problem may explain the disagreement between the actual change in EKE of the western cyclone (about .575 $m^2/s^3$) and the calculated change from the baroclinic conversion and ageostrophic geopotential flux terms only (a net gain of about 8.17 $m^2/s^3$). In this case, the box-integrated method may be underestimating the amount of energy being dispersed near the western cyclone center from net flux divergence. These speculations are supported by the results of the volume integration analysis, as will be presented next.

### *ii) Volume-Integrated Budgets of EKE centers*

As described in Chapter 2, the volume-integrated budgets involved diagnosing the primary EKE tendency terms within three defined EKE centers across the North Pacific basin. To briefly review, the left EKE center was spatially tied to the western cyclone. The central EKE center was positioned downstream of the western cyclone, extending from the Kamchatka Peninsula eastward over the central North Pacific. This energy center predated the existence of the right EKE center and progressively extended further eastward through 00Z 7 October. The right EKE center originated from a split in the central EKE center after 00Z 7 October and became spatially tied to the eastern cyclone. By tracking the evolution of three EKE centers, this study aims to potentially attribute downstream development as a factor in the growth of the eastern cyclone in a manner similar to that suggested by DGS.

Figure 4.7a shows the energy budget for the left EKE center. Interestingly, the primary terms contributed a net sink of EKE before 18Z 6 October as the net ageostrophic geopotential flux divergence was larger than the baroclinic conversion, despite the fact that the magnitude of the left EKE center increased during this time period (refer to Fig. 2.2). This implies that other terms in the EKE tendency equation must have been a factor in developing the left EKE center. After this time, baroclinic conversion outweighed the net ageostrophic geopotential flux divergence until the last time period. The shearwise component of baroclinic conversion was larger than the transverse component at every time step except for the last, where the two components were of nearly equal magnitude. As with the box-integrated results of the western cyclone, the total baroclinic conversion increased through 12Z 7 October. The amount of ageostrophic geopotential flux divergence progressively increased during this time as well, suggesting that as energy was being generated by baroclinic conversion it was subsequently fluxed downstream. The peak growth rate in baroclinic conversion corresponded to the time when the total baroclinic conversion overtook the net ageostrophic geopotential flux divergence (Fig. 4.7b). However, this peak in total baroclinic conversion growth rate did not correspond to a peak in either of the component growth rates. Shearwise baroclinic conversion growth peaked six hours earlier on 12Z 6 October, while the transverse component growth rate peaked much later on 12Z 7 October. Overall, ageostrophic geopotential flux divergence was the dominant tendency term for the left EKE center as revealed by both the volume integrals and growth rates.

Through 12Z 6 October, there was net ageostrophic geopotential flux convergence within the central EKE center (Fig. 4.8a). During this time, the total baroclinic conversion was much smaller, suggesting that the central EKE center primarily grew as a result of convergence of ageostrophic geopotential fluxes emanating from upstream. From 18Z 6 October through the end of the analysis period, the total baroclinic conversion grew larger. This growth was largely a byproduct of the transverse component, as the shearwise component stayed relatively constant and even became slightly negative towards the end of the time period. From 18Z 6 October through 06Z 7 October, net ageostrophic geopotential flux divergence served as a sink of EKE. This time period both immediately preceded and included the development of the right EKE center, suggesting that energy was being fluxed downstream to aid in the development of the right EKE center. After 06Z 7 October, the central EKE center was once again characterized by net ageostrophic geopotential flux convergence as the growth rate of flux divergence decreased (Fig. 4.8b). The growth rate of flux convergence steadily declined from 00Z 6 October through 18Z 6 October, after which it began to rise again. Overall, the pattern of growth rates for the total and component baroclinic conversion terms mirrored that of the volume integrals. Thus, the evolution of the central EKE center was mostly dominated by ageostrophic geopotential fluxes, serving as an intermediary between the left and right EKE centers.

After its inception on 06Z 7 October, the right EKE center grew almost entirely from net ageostrophic geopotential flux convergence (Fig. 4.9a). Similar to the box-integrated results of the eastern cyclone, the total baroclinic conversion was negative largely due to the shearwise component being negative, though the transverse component was slightly negative as well. As the total baroclinic conversion became less of a sink of EKE towards the end of the analysis period, the amount of ageostrophic geopotential flux divergence gradually increased. This also coincided with an increase in the geopotential flux convergence, such that the right EKE center was able to continue to grow at a rapid rate in association with the eastern cyclone's development. The growth rate of ageostrophic geopotential flux convergence peaked on 06Z 7 October, but otherwise the evolution of the growth rates of the other tendency terms mostly mirrored that of the volume integrals (Fig. 4.9b). Given these results, it is fair to argue that the development of the eastern cyclone was a case of downstream development as defined by DGS. That is, there was a period of time (06Z through 12Z 7 October) when the right EKE center grew primarily as a result of ageostrophic geopotential flux convergence. This was preceded by a time period (00Z through 12Z 6 October) when the central EKE center positioned upstream also grew from ageostrophic geopotential flux convergence.

Thus, the volume integrated budgets of the left and right EKE centers show that the shearwise component of baroclinic conversion was a significant factor in determining the overall progression of the total baroclinic conversion term. For the left EKE center, the shearwise component was dominant at almost every time step, similar to the results of the box integral associated with the western cyclone. Meanwhile, the right EKE center was characterized by initially negative total baroclinic conversion characterized by a strongly negative shearwise component, similar to the results of the eastern cyclone box integral. Moreover, the rapid development of the eastern cyclone in spite of initially negative baroclinic conversion seems to have been tied to energy dispersed downstream from the western cyclone. The central EKE center was defined by a more transverse-dominant component of baroclinic conversion in contrast to the other two EKE centers, but was not directly tied to a developing surface cyclone. Therefore, results from both the box-integrated and volume-integrated methods suggest that shearwise vertical motions may contribute a significant portion of the total vertical motions involved in the baroclinic conversion process associated with developing surface cyclones. The next section will offer an analysis as to why this may be.

## c. Vertical Cross-Sections of Baroclinic Conversion

### *i) Results of Vertical Cross-Sections*

To diagnose possible reasons why the shearwise baroclinic conversion tended to be larger in this case study, vertical cross-sections were taken in the vicinity of each storm at a selected time. Such an analysis identifies where the vertical motions and associated baroclinic conversion were strongest in the atmospheric column, offering clues as to whether lower-tropospheric and/or upper-tropospheric processes were predominant in driving the baroclinic conversion process. The cross-sections were taken through the areas of maximum vertically-integrated baroclinic conversion along a line perpendicular to the long axes of the left and right EKE centers, which were associated with the developments of the western and eastern cyclones, respectively. Each of the cross-sections were taken on 06Z 7 October as this analysis time represented the end of a period of explosive cyclogenesis for each cyclone as defined by Sanders and Gyakum (1980). For reference, Fig. 4.10 shows the locations of each cross-section.

Figure 4.11 shows the vertical cross-section taken in association with the western cyclone. From this perspective, it is clear that the maximum baroclinic conversion was occurring in the upper troposphere around 350 hPa (Fig. 4.11a). This was near the location of the warmest temperature anomalies, which were maximized around 375 hPa. Further above the area of maximum positive baroclinic conversion, there was an area of negative baroclinic conversion co-located with cold temperature anomalies near 200 hPa. Examining the partitioned components of baroclinic conversion reveals that the shearwise baroclinic conversion was more concentrated near the maximum in total baroclinic conversion around 350 hPa (Fig. 4.11b). Meanwhile, the maximum in transverse baroclinic conversion was more diffuse throughout the upper troposphere, extending from near 300 hPa to near 500 hPa. The fact that the shearwise baroclinic conversion was co-located with the vertical level of the maximum perturbation temperatures may hint at some of the reasoning behind why the shearwise baroclinic conversion was so predominant in the development of the western cyclone. That is, if the shearwise vertical motions were more vertically aligned with the distribution of perturbation temperatures, that would account for a greater contribution towards the total baroclinic conversion as the calculation of $-\omega\alpha$ would be larger. Figure 4.11c shows that this was indeed the case as the shearwise vertical motions peaked in the upper troposphere around 350 hPa, whereas the transverse vertical motions were more concentrated in the lower troposphere around 800 hPa.

A similar scenario is revealed by examining the vertical cross-section taken in association with the eastern cyclone (Fig. 4.12). The peak in the negative total baroclinic conversion occurred around 350 hPa (Fig. 4.12a). Although the peak in cold temperature anomalies occurred lower in the troposphere around 600 hPa, there was a secondary maximum in cold anomalies around 350 hPa. The shearwise component of baroclinic conversion also exhibited two separate maxima nearly co-located with the peaks in the cold temperature anomalies (Fig. 4.12b). In contrast, the negative transverse baroclinic conversion only had one maxima in the upper troposphere around 350 hPa. However, there was actually an area of positive transverse baroclinic conversion around 600 hPa. Examining the vertical motions directly reveals that the shearwise vertical motions peaked between 350 hPa and 600 hPa, whereas the transverse vertical motions were maximized around 800 hPa (Fig. 4.12c).

Thus, analysis of the vertical cross-sections suggests that the shearwise vertical motions associated with the development of each cyclone were more in phase with the vertical distribution of temperature anomalies than were the transverse vertical motions. Specifically, the shearwise vertical motions tended to peak in the upper troposphere along with the temperature anomalies, whereas the transverse vertical motions were more concentrated in the lower troposphere. Such a combination would provide an explanation as to why the shearwise baroclinic conversion was predominant in the evolution of the total baroclinic conversion. Furthermore, this suggests that baroclinic conversion occurring in the upper troposphere contributed more to the total atmospheric column baroclinic conversion than that which occurred in the lower troposphere. The following subsection will examine this possibility in more detail.

### *ii) Vertical Partitioning of the Baroclinic Conversion Term*

In order to diagnose whether the baroclinic conversion process was favored in the upper troposphere, the total vertically-averaged baroclinic conversion was split into three separate layers bounded by pressure surfaces. The total, shearwise, and transverse baroclinic conversion were then vertically averaged within each of these layers in order to compare contributions to the total atmospheric column baroclinic conversion from each layer. The three layers consisted of: 1) A “lower” layer, which extended from 950 hPa to 750 hPa, 2) a “middle” layer, which extended from 750 hPa 450 hPa, and 3) an “upper” layer, which extended from 450 hPa to 150 hPa. The bounding levels for the lower layer were chosen to capture the baroclinic conversion that was occurring predominately in the lower troposphere, while the middle layer bounds were chosen to describe the baroclinic conversion occurring in the middle and upper troposphere. The upper layer bounds were chosen to capture the remaining baroclinic conversion that was occurring in the upper troposphere and parts of the lower stratosphere. Finally, the vertically-partitioned baroclinic conversion calculations at each grid point were horizontally integrated using the box method as described previously in order to asses the results associated with each cyclone.

The results of this analysis reveal that most of the baroclinic conversion associated with the western cyclone was performed in the middle layer (Fig. 4.13a). In fact, the baroclinic conversion that occurred in the middle layer was even greater than the total atmospheric column baroclinic conversion, which was almost equivalent to the total baroclinic conversion that occurred in the upper layer. This was likely due to the fact that the vertical averaging within the upper layer included the negative baroclinic conversion that was occurring in the lower stratosphere (refer back to Fig. 4.11a). This area of negative baroclinic conversion was not included in the vertical averaging of the middle layer, such that the total baroclinic conversion occurring within the middle layer ended up exceeding the calculated total baroclinic conversion occurring in the upper layer and the total atmospheric column. Meanwhile, the lower layer contributed very little baroclinic conversion compared to the middle and upper layers.

Examining the partitioned components of baroclinic conversion within each layer, it is clear that the shearwise baroclinic conversion was predominant in the upper layer throughout the entire analysis period (Fig. 4.13b). In fact, after 00Z 7 October, the shearwise baroclinic conversion was more than twice as large as the transverse baroclinic conversion in the upper layer. The middle layer was characterized by a more even split between the shearwise and transverse components (Fig. 4.13c). Before 18Z 6 October, the shearwise baroclinic conversion was predominant, whereas the transverse baroclinic conversion was predominant after this time. Overall, however, the shearwise and transverse components in the middle layer were much closer to one another in magnitude than the component portions were in the upper layer. In contrast, the transverse baroclinic conversion dominated in the lower layer during most of the case study (Fig. 4.13d). The shearwise component was slightly larger than the transverse component through 12Z 6 October, but by 06Z 7 October the transverse component was more than twice as large as the shearwise component.

The upper layer contributed most of the negative baroclinic conversion to the eastern cyclone (Fig. 4.14a), whereas the middle layer contributed negative baroclinic conversion through 18Z 6 October but then became the largest source of positive baroclinic conversion thereafter. The shift in the total column baroclinic conversion from being negative to positive coincided with the large increase in positive baroclinic conversion occurring in the middle layer. Meanwhile, the lower layer baroclinic conversion was positive throughout the case study and thus helped to offset the negative contributions from the middle and upper layers during the early stages of the eastern cyclone's development.

As with the western cyclone, the shearwise baroclinic conversion dominated the evolution of the upper layer baroclinic conversion with the eastern cyclone (Fig. 4.14b). Whereas the shearwise component was negative throughout the analysis time period, the transverse component oscillated between being positive and negative and was smaller in overall magnitude until 18Z 7 October. The progression of the middle layer was more complex (Fig. 4.14c). The shearwise component predominated as the total baroclinic conversion was negative through 18Z 6 October, but thereafter the transverse baroclinic conversion dominated as the total baroclinic conversion became positive. Overall, the transverse baroclinic conversion was positive throughout the entire case study in the middle layer, whereas the shearwise component did not become positive until after 06Z 7 October. In the lower layer, the shearwise baroclinic conversion was negative and exhibited a large influence on the total baroclinic conversion through 18Z 6 October (Fig. 4.14d). After this time, the total baroclinic conversion became more positive as the transverse component predominated.

Thus, this additional analysis suggests that baroclinic conversion occurring in both the middle and upper troposphere contributed the most to the total column baroclinic conversion for both the western and eastern cyclones. In addition, shearwise vertical motions occurring in these layers seemed to contribute more to the total baroclinic conversion than the transverse vertical motions, which were more predominant in the lower troposphere. This suggests that shearwise vertical motions occurring in the middle and upper troposphere may be responsible for the overall dominance of the shearwise baroclinic conversion in association with both cyclones.

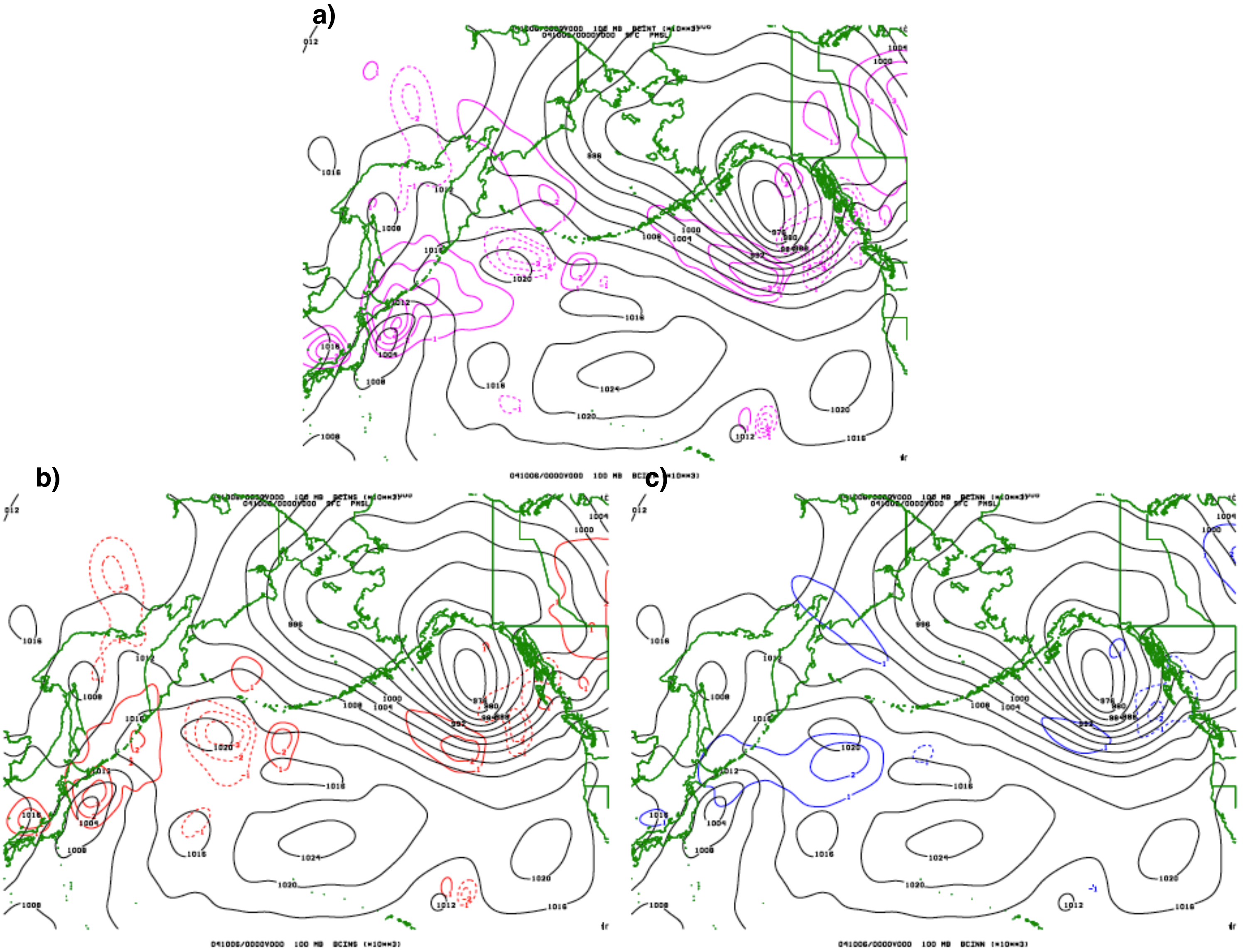

**Figure 4.1: a)** Positive (solid pink) and negative (dashed pink) vertically-averaged total baroclinic conversion contoured every 1 $m^2/s^3$ and scaled by a factor of $10^3$, and mean sea-level pressure (solid black) contoured every 4 hPa, on 00Z 6 October. **b)** Positive (solid red) and negative (dashed red) vertically-averaged shearwise component of baroclinic conversion contoured every 1 $m^2/s^3$ and scaled by a factor of $10^3$, and mean sea-level pressure (solid black) contoured every 4 hPa, on 00Z 6 October. **c)** Positive (solid blue) and negative (dashed blue) vertically-averaged transverse component of baroclinic conversion contoured every 1 $m^2/s^3$ and scaled by a factor of $10^3$, and mean sea-level pressure (solid black) contoured every 4 hPa, on 00Z 6 October.

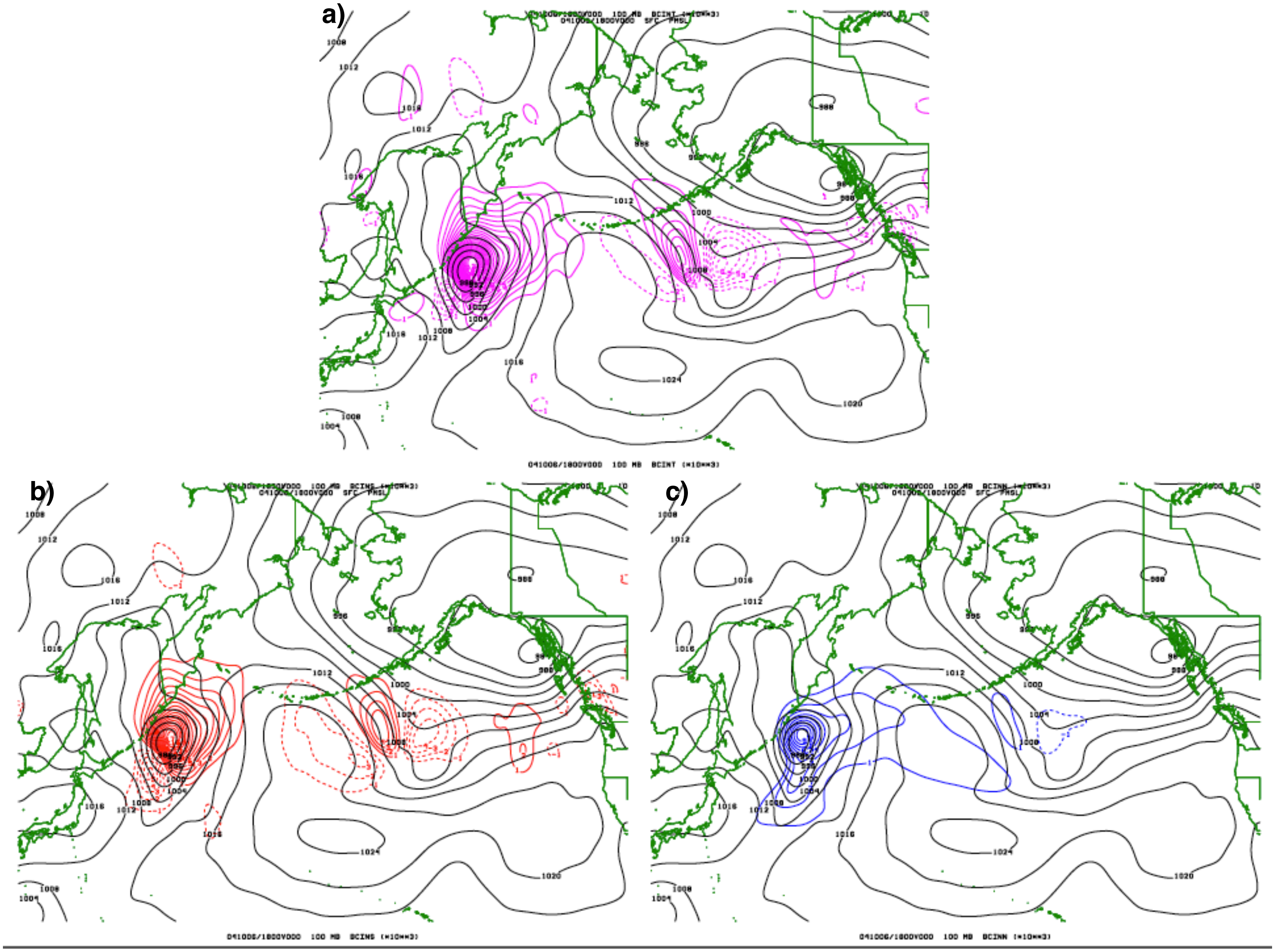

**Figure 4.2: a)** As for Fig. 4.1a, except on 18Z 6 October. **b)** As for Fig. 4.1b, except on 18Z 6 October. **c)** As for Fig. 4.1c, except on 18Z 6 October.

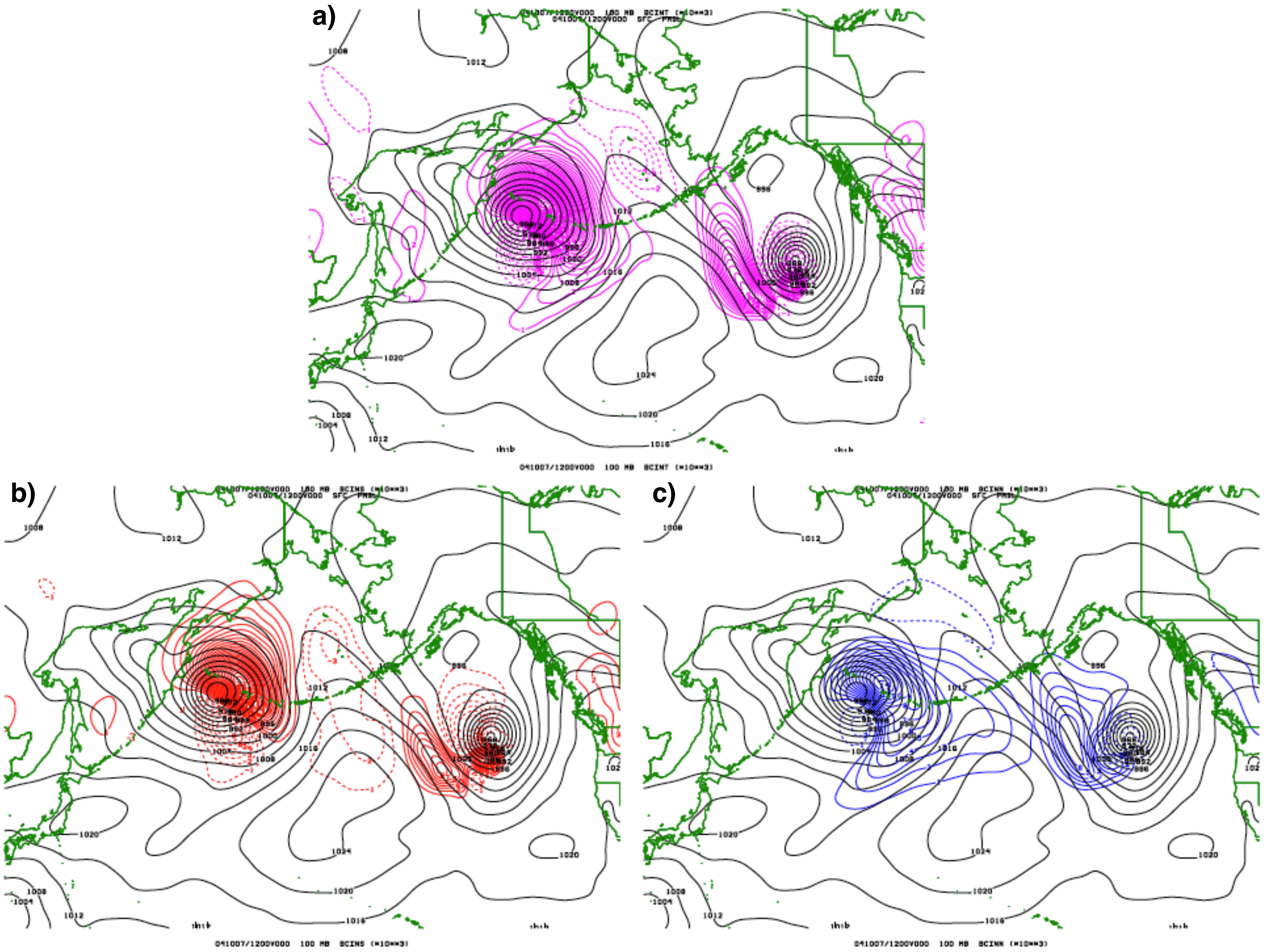

**Figure 4.3: a)** As for Fig. 4.1a, except on 12Z 7 October. **b)** As for Fig. 4.1b, except on 12Z 7 October. **c)** As for Fig. 4.1c, except on 12Z 7 October.

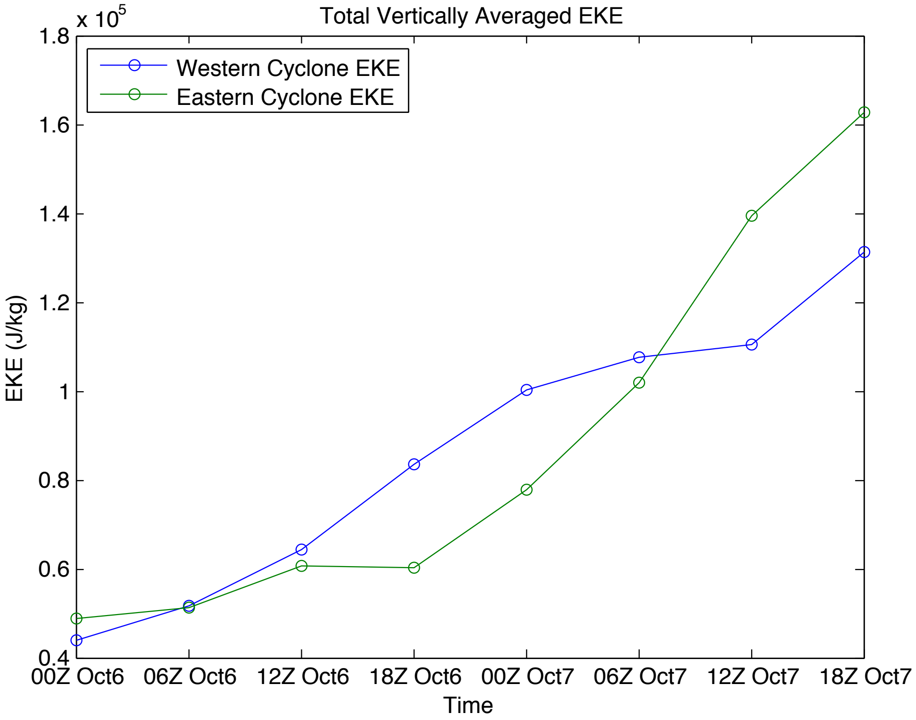

**Figure 4.4:** Vertically-averaged Eddy Kinetic Energy in J/Kg plotted as a function of analysis time for the western (solid blue) and eastern (solid green) cyclones.

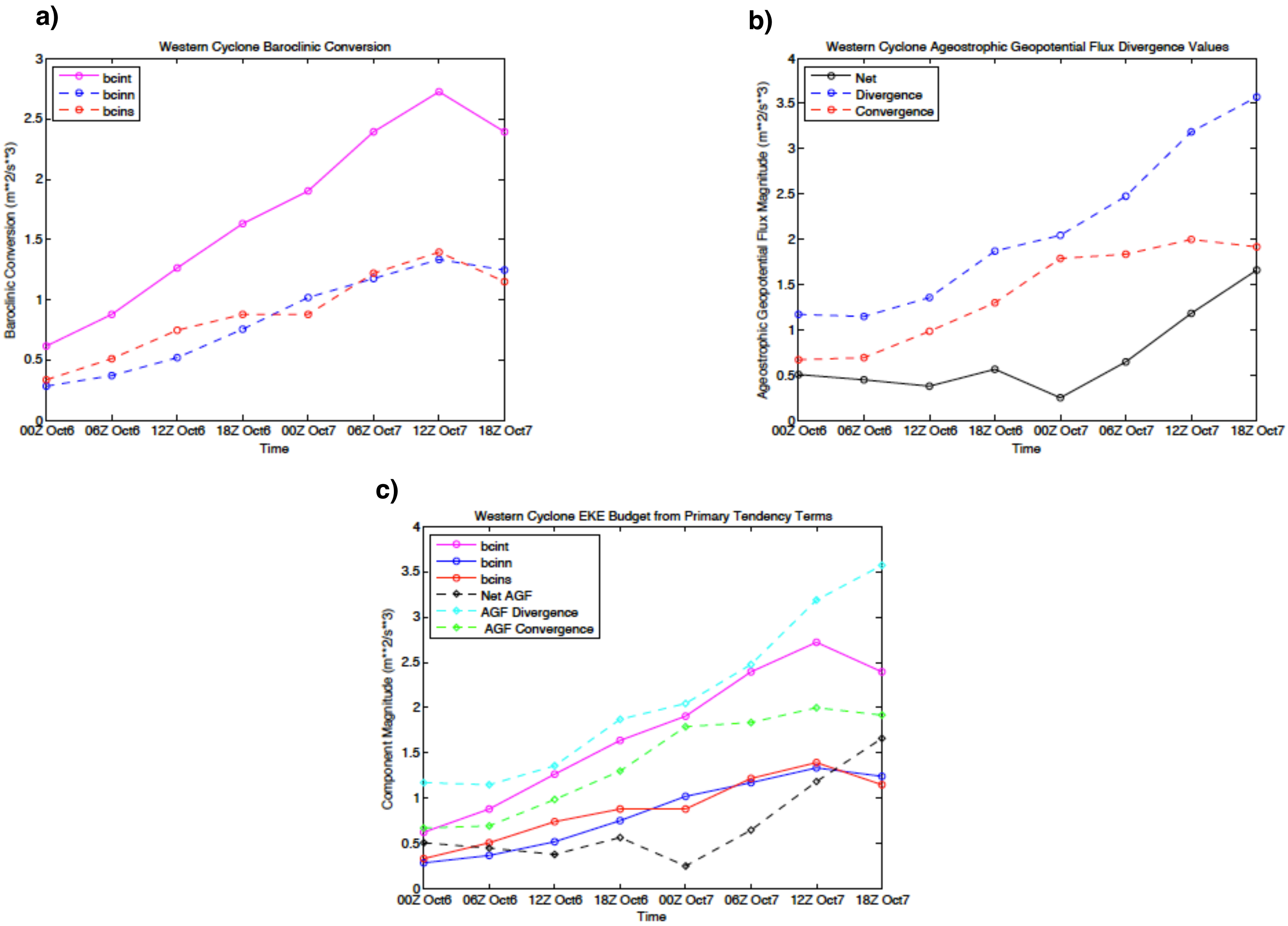

**Figure 4.5: a)** Box-integrated total (solid pink), shearwise (dashed red), and transverse (dashed blue) vertically-averaged baroclinic conversion in $m^2/s^3$ plotted as a function of analysis time for the western cyclone. **b)** Box-integrated net (solid black), convergent (dashed red), and divergent (dashed blue) vertically-averaged ageostrophic geopotential fluxes in $m^2/s^3$ plotted as a function of analysis time for the western cyclone. **c)** Box-integrated magnitudes of the primary tendency terms, including total (solid pink), shearwise (solid red) and transverse (solid blue) vertically-averaged baroclinic conversion as well as net (dashed black), convergent (dashed green), and divergent (dashed teal) vertically-averaged ageostrophic geopotential fluxes in $m^2/s^3$ plotted as a function of analysis time for the western cyclone.

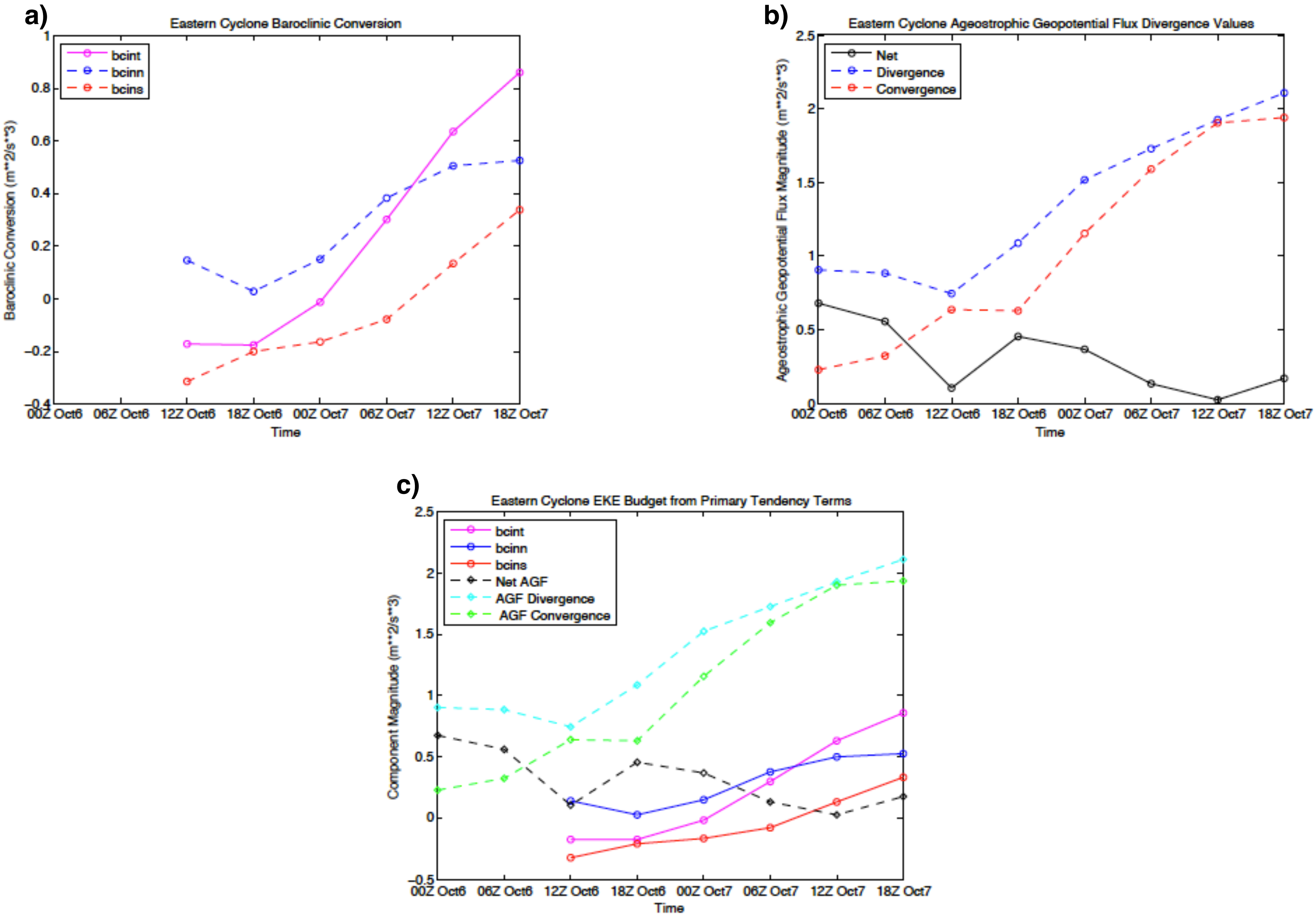

**Figure 4.6: a)** As for Fig. 4.5a, but for the eastern cyclone. **b)** As for Fig. 4.5b, but for the eastern cyclone. **c)** As for Fig. 4.5c, but for the eastern cyclone.

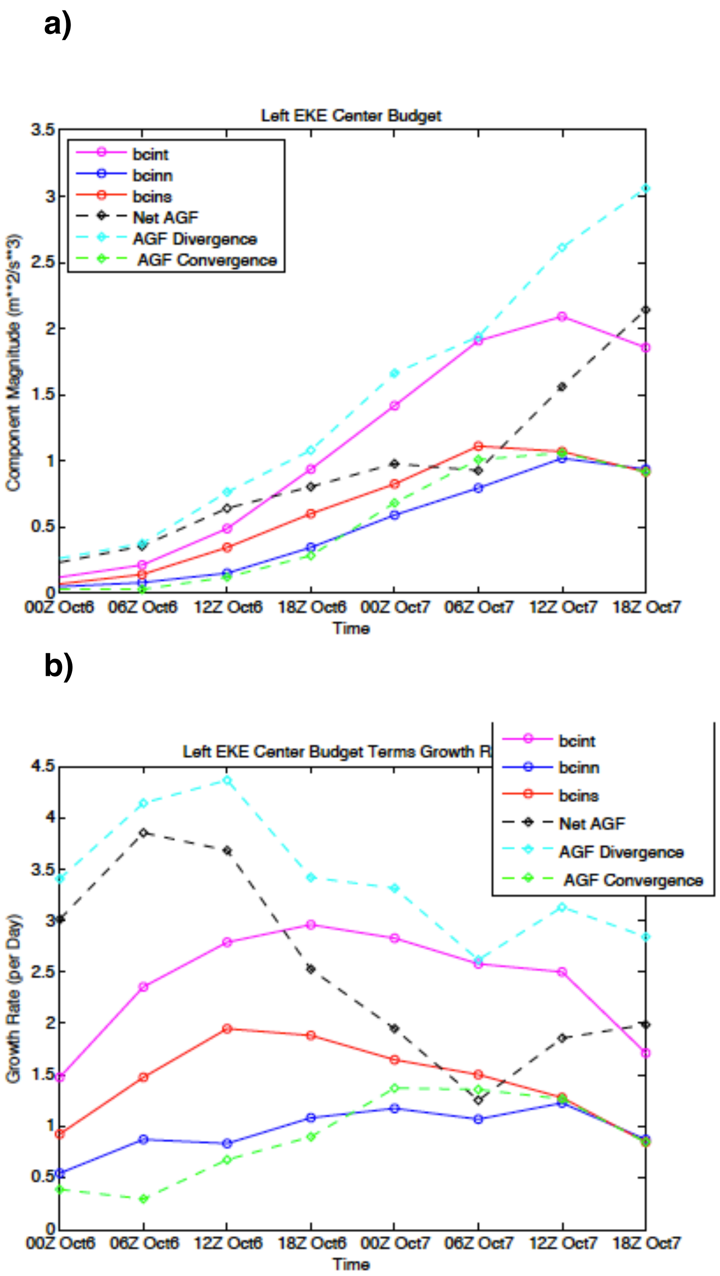

**Figure 4.7: a)** Volume-integrated magnitudes of the primary tendency terms, including total (solid pink), shearwise (solid red) and transverse (solid blue) vertically-averaged baroclinic conversion as well as net (dashed black), convergent (dashed green), and divergent (dashed teal) vertically-averaged ageostrophic geopotential fluxes in $m^2/s^3$ plotted as a function of analysis time for the left EKE center. **b)** As for Fig. 4.7a, but expressed in terms of a growth rate per day.

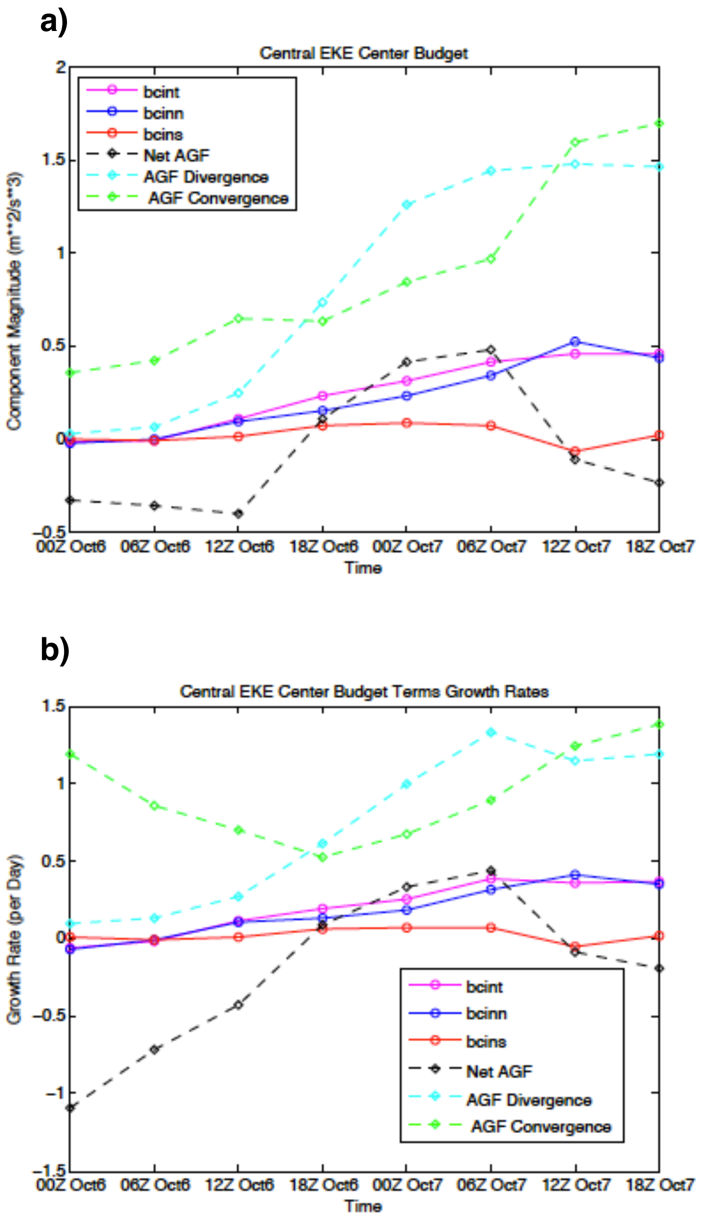

**Figure 4.8: a)** As for Fig. 4.7a, except for the central EKE center. **b)** As for Fig. 4.7b, but for the central EKE center.

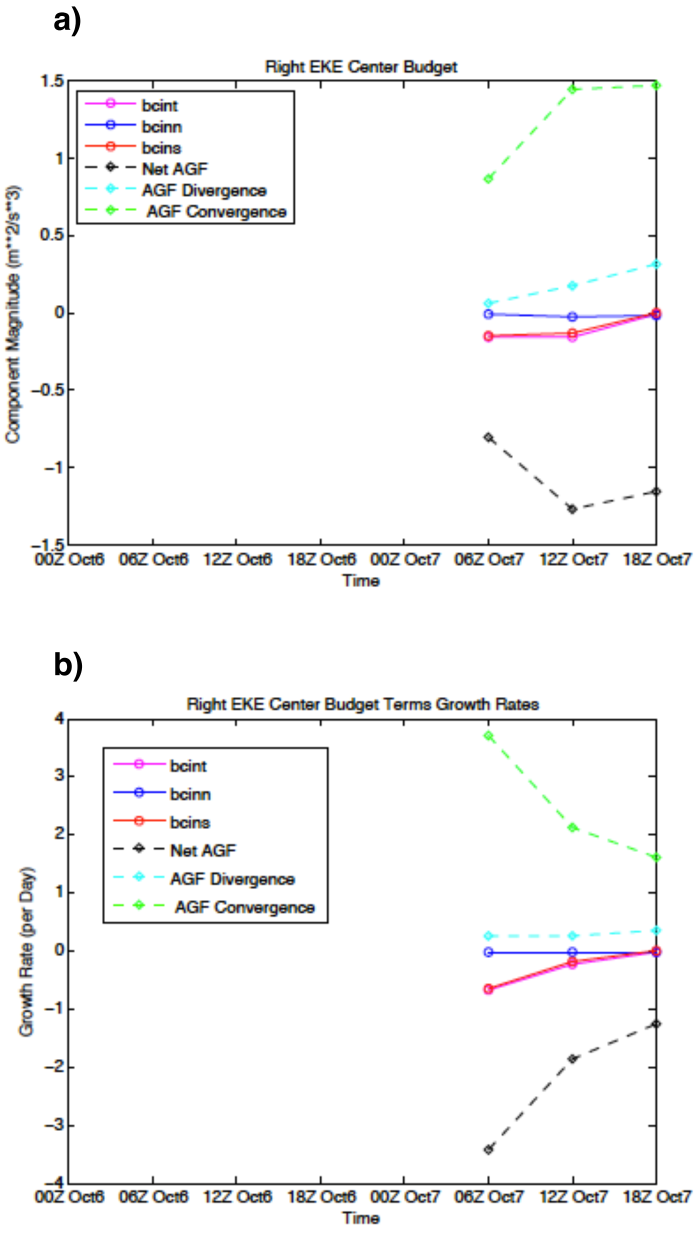

**Figure 4.9: a)** As for Fig. 4.7a, except for the right EKE center. **b)** As for Fig 4.7b, but for the right EKE center.

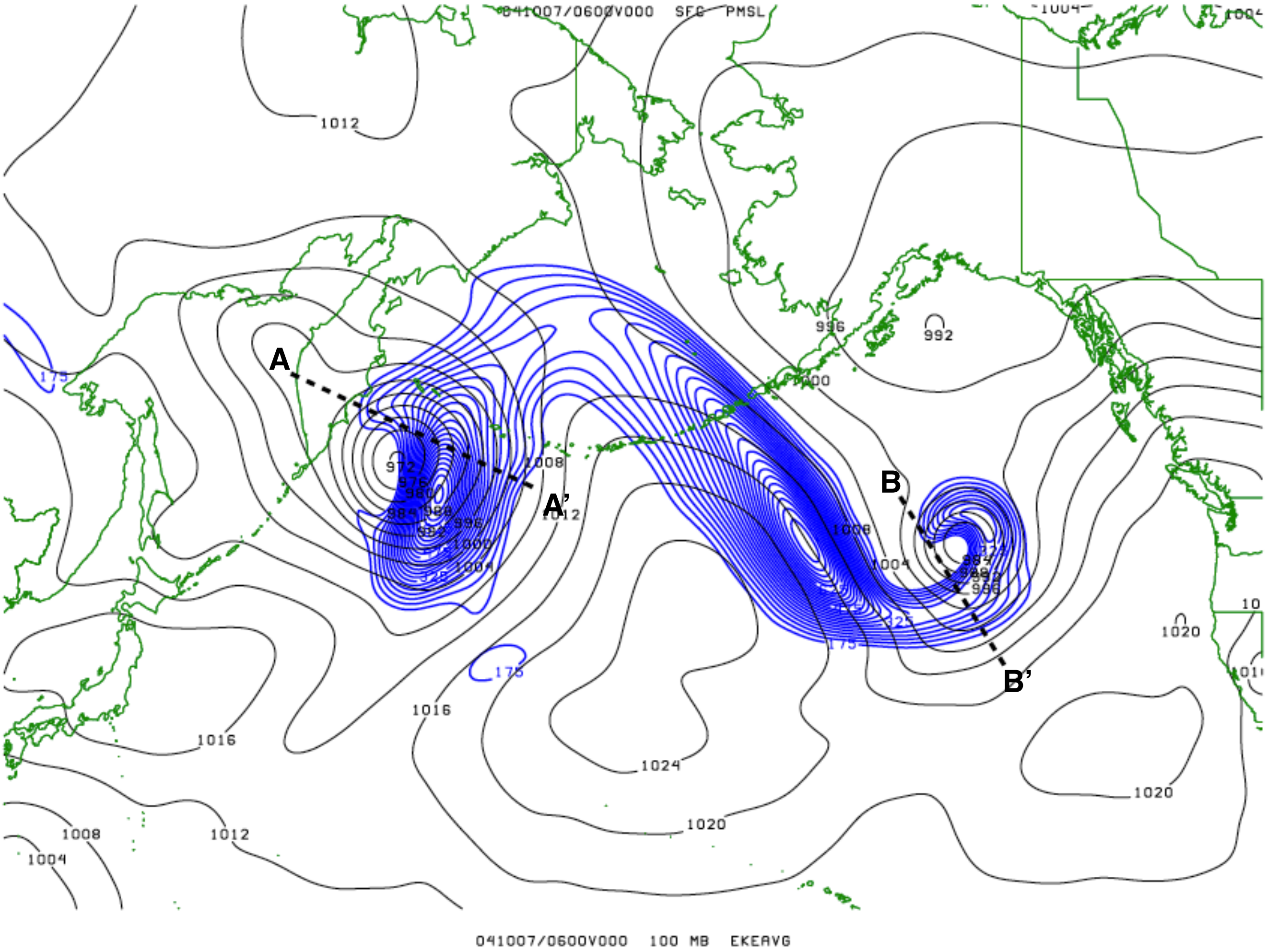

**Figure 4.10:** Vertically averaged EKE (solid blue) contoured every 25 $m^2/s^2$ beginning with 175 $m^2/s^2$, and mean sea-level pressure (solid black) contoured every 4 hPa, on 06Z 7 October. Bold, dashed black lines delineate the locations of the vertical cross-sections taken in accordance with the western and eastern cyclones.

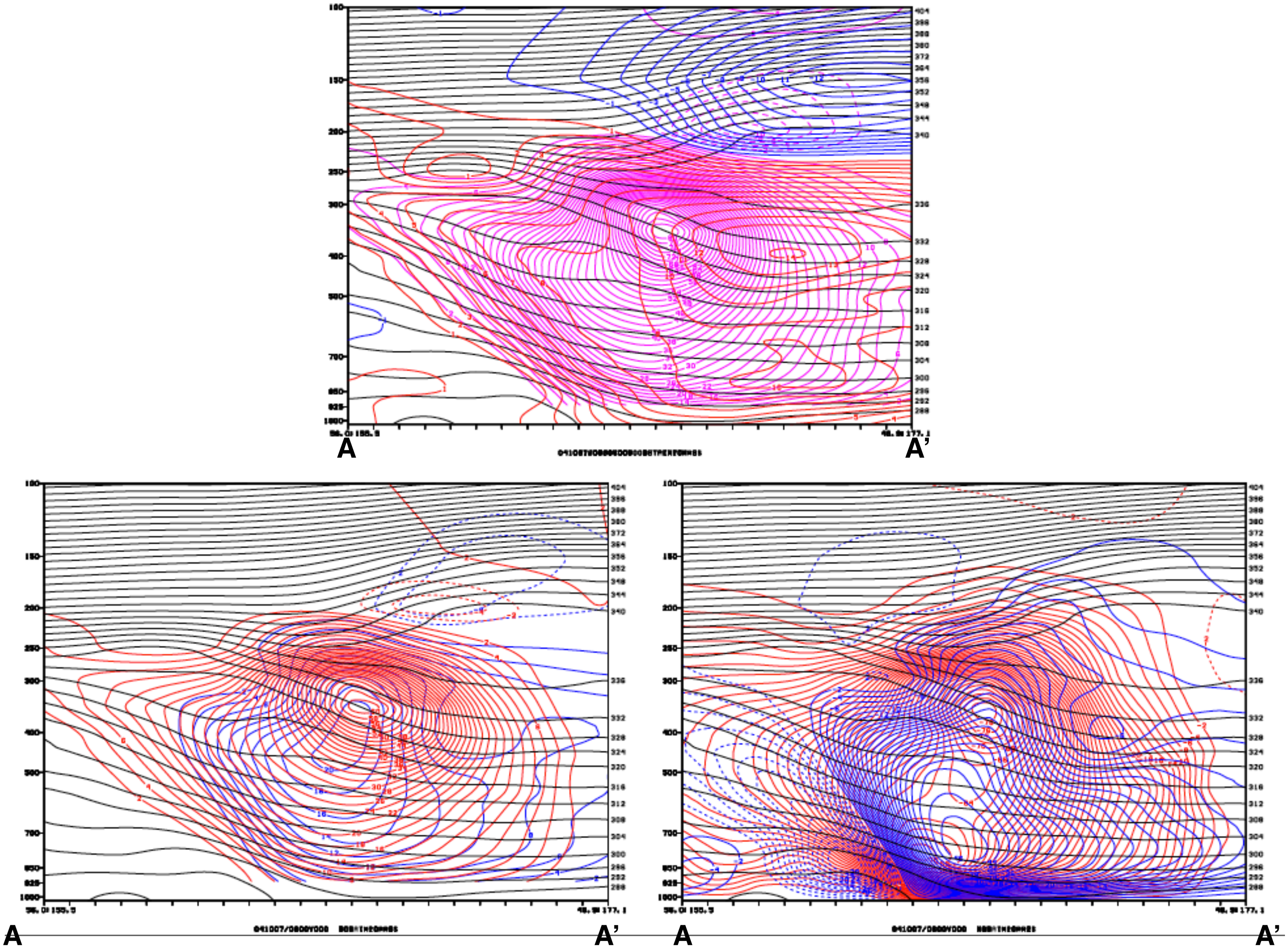

**Figure 4.11: a)** Vertical cross-section taken along the line from A to A' shown in fig. 10 through the western cyclone of potential temperature (solid black) contoured every 4 K, perturbation warm (red) and cold (blue) temperature anomalies contoured every 1 K, and total (pink) baroclinic conversion contoured every 2 $m^2/s^3$ and scaled by a factor of $10^3$, shown on 06Z 7 October. Positive (negative) values are shown with solid (dashed) contours. **b)** Vertical cross-section taken along the same line as in Fig. 4.11a showing potential temperature (solid black) contoured every 4 K, and shearwise (red) and transverse (blue) baroclinic conversion contoured every 2 $m^2/s^3$ and scaled by a factor of $10^3$, shown on 06Z 7 October. Positive (negative) values are shown with solid (dashed) contours. **c)** Vertical cross-section taken along the same line as in Fig. 4.11a showing potential temperature (solid black) contoured every 4 K, and the shearwise (red) and transverse (blue) components of the quasi-geostrophic vertical motion contoured every 2 Pa/s beginning at 2 Pa/sec and scaled by a factor of $10^2$, shown on 06Z 7 October. Regions of ascent (descent) are shown with solid (dashed) contours.

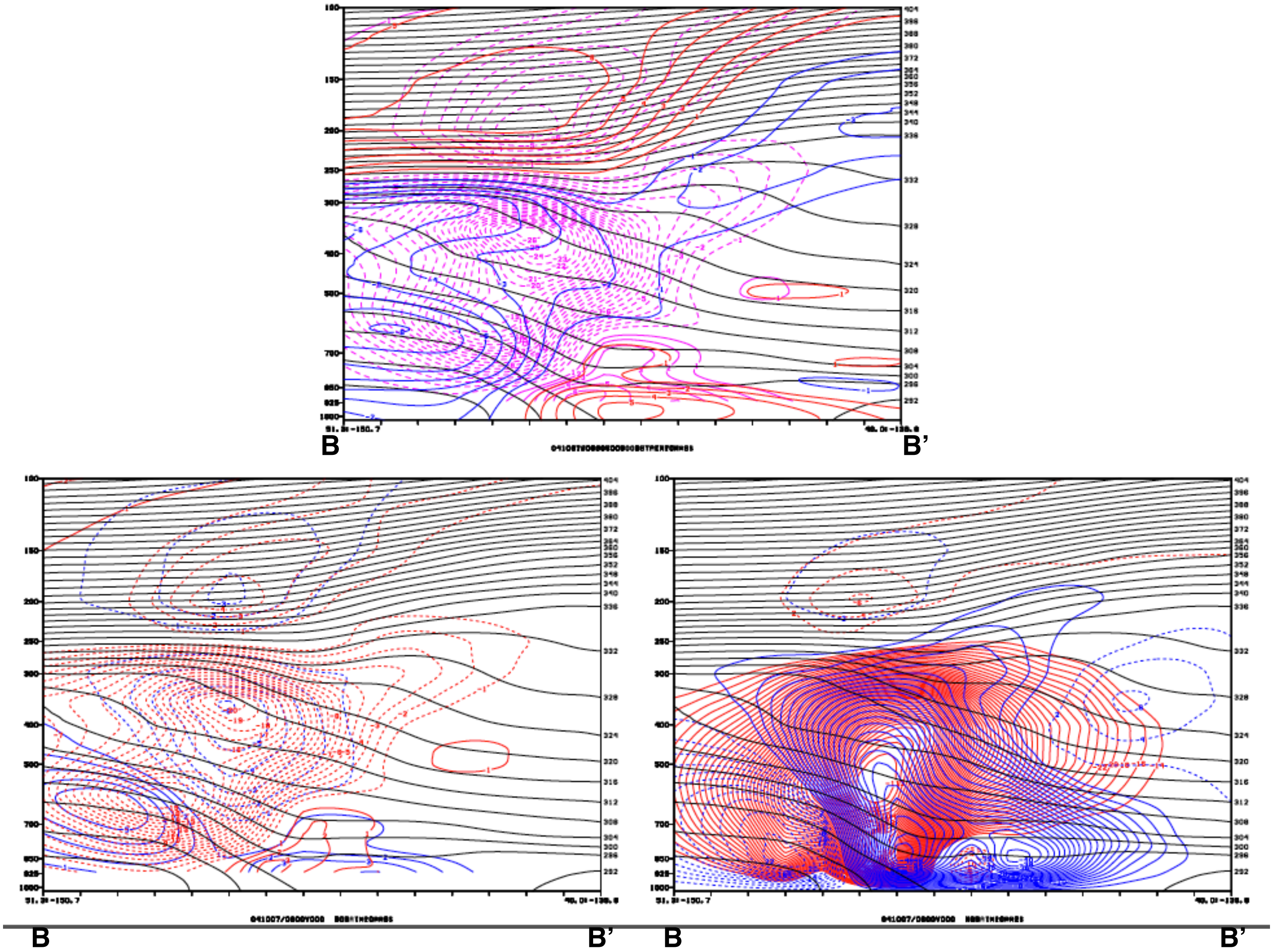

**Figure 4.12: a)** Vertical cross-section taken along the line from B to B’ shown in Fig. 4.10 through the eastern cyclone of potential temperature (solid black) contoured every 4 K, perturbation warm (red) and cold (blue) temperature anomalies contoured every 1 K, and total (pink) baroclinic conversion contoured every 1 $m^2/s^3$ and scaled by a factor of $10^3$, shown on 06Z 7 October. Positive (negative) values are shown with solid (dashed) contours. **b)** Vertical cross-section taken along the same line as in Fig. 4.12a showing potential temperature (solid black) contoured every 4 K, and shearwise (red) and transverse (blue) baroclinic conversion contoured every 1 $m^2/s^3$ and scaled by a factor of $10^3$, shown on 06Z 7 October. Positive (negative) values are shown with solid (dashed) contours. **c)** Vertical cross-section taken along the same line as in Fig. 4.12a showing potential temperature (solid black) contoured every 4 K, and the shearwise (red) and transverse (blue) components of the quasi-geostrophic vertical motion contoured every 2 Pa/s beginning at 2 Pa/sec and scaled by a factor of $10^2$, shown on 06Z 7 October. Regions of ascent (descent) are shown with solid (dashed) contours.

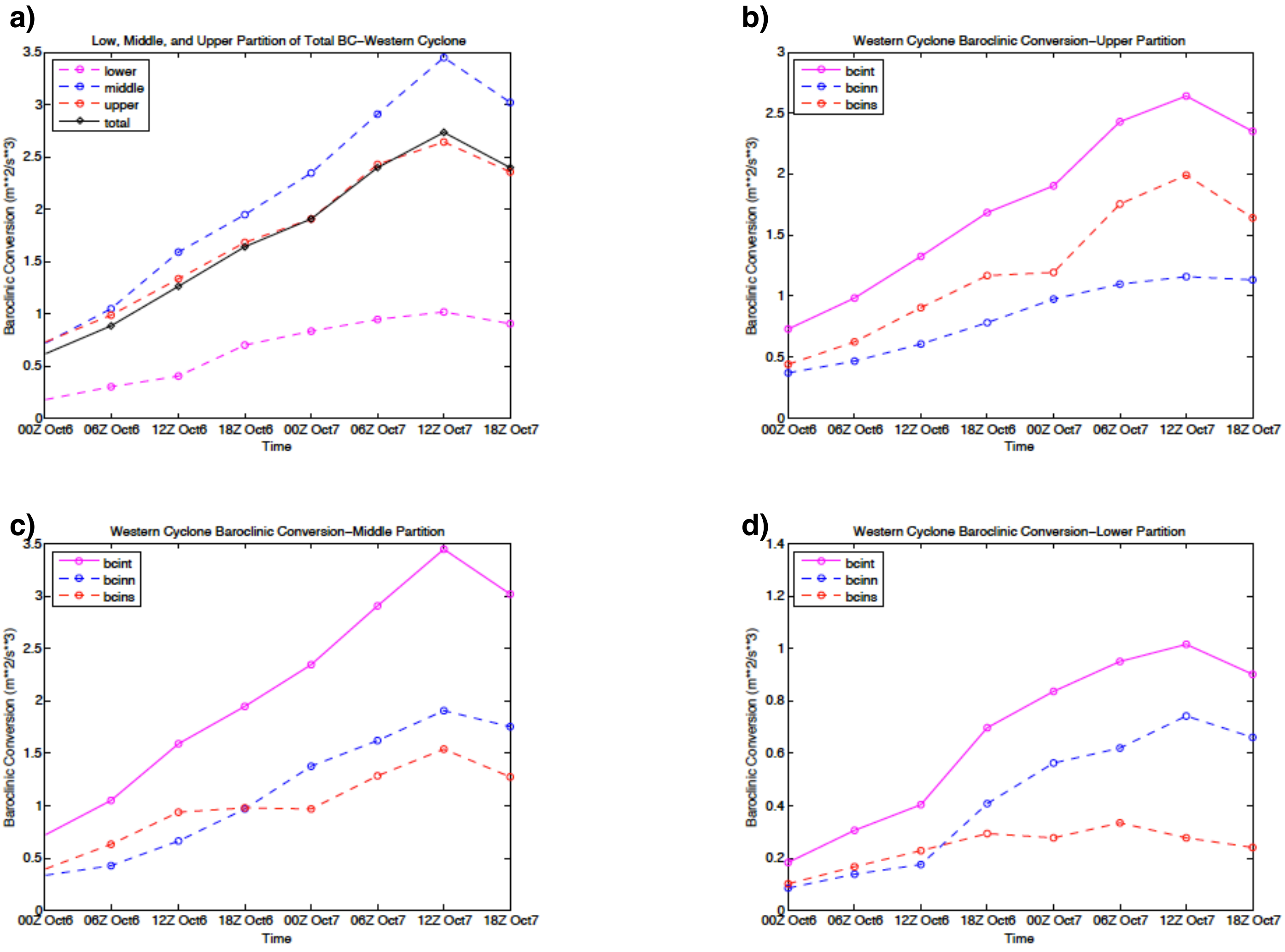

**Figure 4.13: a)** Box-integrated total column (solid black), lower (dashed pink), middle (dashed blue), and upper (dashed red) layer total baroclinic conversion in $m^2/s^3$ plotted as a function of analysis time for the western cyclone. **b)** Box-integrated total (solid pink), shearwise (dashed red), and transverse (dashed blue) vertically-averaged baroclinic conversion in $m^2/s^3$ occurring in the upper layer plotted as a function of analysis time for the western cyclone. **c)** Box-integrated total (solid pink), shearwise (dashed red), and transverse (dashed blue) vertically-averaged baroclinic conversion in $m^2/s^3$ occurring in the middle layer plotted as a function of analysis time for the western cyclone. **d)** Box-integrated total (solid pink), shearwise (dashed red), and transverse (dashed blue) vertically-averaged baroclinic conversion in $m^2/s^3$ occurring in the lower layer plotted as a function of analysis time for the western cyclone.

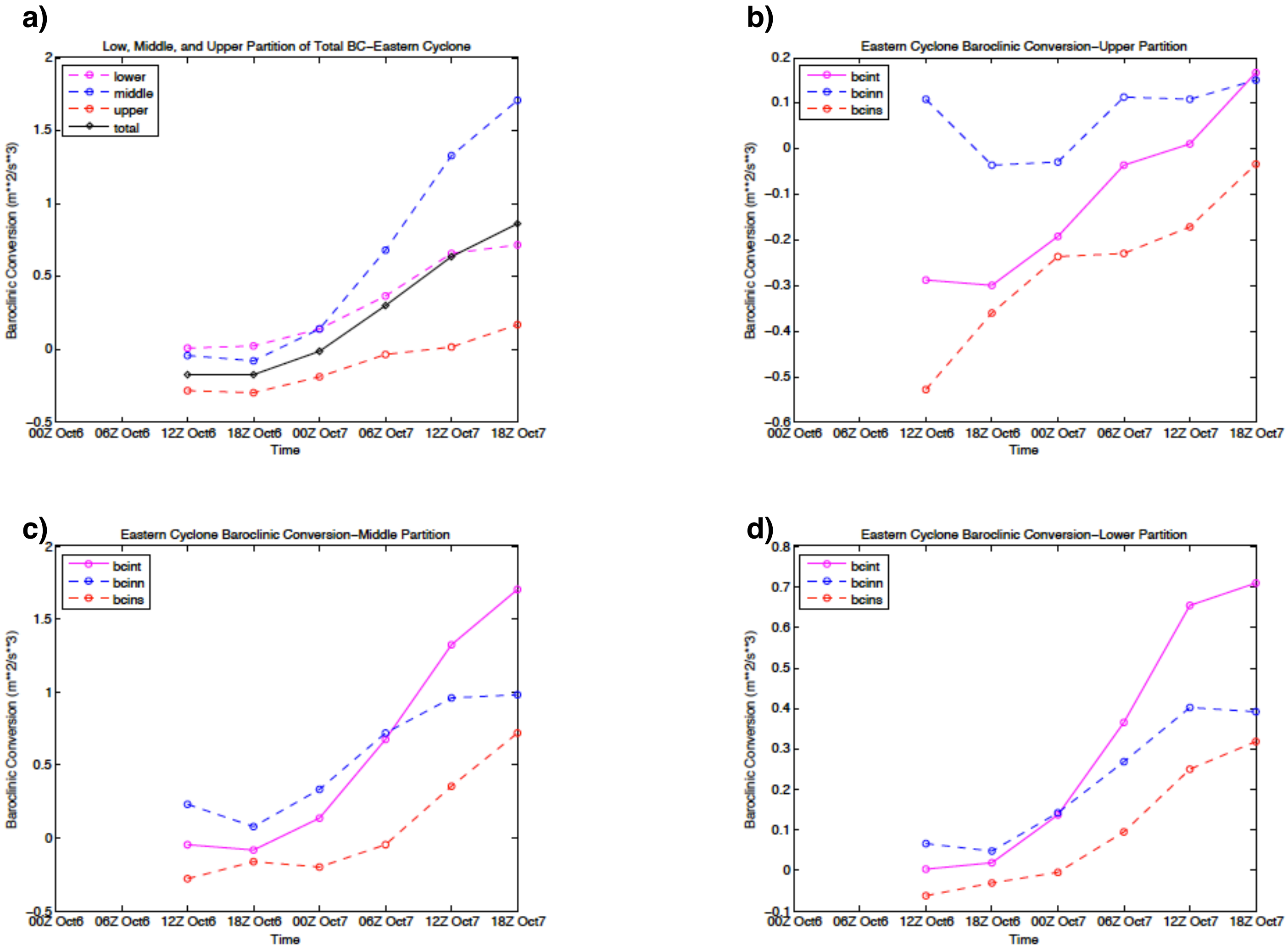

**Figure 4.14: a)** As for Fig. 4.13a, but for the eastern cyclone. **b)** As for Fig. 4.13b, but for the eastern cyclone. **c)** As for Fig. 4.13c, but for the eastern cyclone. **d)** As for Fig. 4.13d, but for the eastern cyclone.

# Chapter 5: Discussion

## a. Review

The development of extratropical cyclones has historically been considered from a variety of perspectives. The local energetics perspective has served to quantify the evolution of the EKE associated with baroclinic disturbances. Pioneering work by Orlanski and Sheldon (1995) developed a downstream development paradigm within which baroclinic disturbances could be generated in part through the dispersion of energy from upstream systems. Within this paradigm, energy is dispersed downstream through ageostrophic geopotential fluxes, which converge in a new location to foster the development of a new disturbance. As the disturbance matures, the process of baroclinic conversion contributes to the production of EKE as a thermally direct vertical circulation converts atmospheric available potential energy into EKE. In most cases, the divergence of ageostrophic geopotential fluxes and the process of baroclinic conversion are the main mechanisms that control the evolution of EKE associated with a disturbance (McLay and Martin, 2002). Recent work utilizing the local energetics perspective has attempted to document the role of these terms with regards to the development of mid-latitude cyclones. DGS examined the relationship between downstream development and North Pacific extra-tropical cyclones and found that about half of the cyclones that developed over the East Pacific during their study could be characterized as an example of downstream development. Meanwhile, modeling studies by Schemm et al. (2013) and Papritz and Schemm (2013) also illustrated the effects of downstream development in the formation of extra-tropical disturbances.

Other investigations into mid-latitude cyclogenesis have followed a more traditional perspective utilizing QG diagnostics. New insights into the development of extra-tropical cyclones have been gleaned by partitioning the QG vertical motion into shearwise and transverse components following the work of Keyser et al. (1992). Martin (1999) found that ascent in the occluded portion of cyclones was largely driven by shearwise vertical motions, with later work showing that shearwise vertical motions were also predominant in the origin and intensification of the lower-tropospheric cyclone structure (Martin 2006, 2007). Studies examining precursors to cyclogenesis, such as upper-front systems, have also found that shearwise vertical motions play a predominant role in the development of these disturbances (Lang and Martin 2010, 2012a, 2012b). While previous work has emphasized the role of the “Shapiro effect” in the creation of upper-fronts, Martin (2014) showed that shearwise vertical motions diagnosed by geostrophic vorticity advection by the thermal wind play a dominant role in generating these systems.

The goal of this study has been to combine the local energetics perspective with the partitioning of QG vertical motions in the hopes of gaining new insights into the energetic development of extra-tropical cyclones. Specifically, deeper investigation of the baroclinic conversion term was performed since, in the absence of Reynolds stress, baroclinic conversion is the only term that can directly generate EKE rather than simply redistribute it. Baroclinic conversion inherently relies on vertical motions being non-zero, which makes the application of partitioned vertical motions to the study of the baroclinic conversion process potentially insightful. Given that transverse vertical motions are a direct manifestation of thermally direct/indirect vertical circulations, it was hypothesized that transverse vertical motions would dominate shearwise vertical motions with regards to the baroclinic conversion process. This would provide an interesting contrast between cyclone energetics and QG perspectives of cyclogenesis as different species of vertical motion would play predominant roles in the evolution of EKE associated with baroclinic disturbances and the development of extra-tropical cyclones.

To investigate this hypothesis, a case study of two cyclones that developed nearly simultaneously across the North Pacific during early October 2004 was considered. The first of this pair of surface cyclones began to develop over the West Pacific on 00Z 6 October, while the second system began to develop to the east approximately 12 hours later. Both cyclones qualified as “bombs” (defined by Sanders and Gyakum, 1980), as the MSLP of each system eventually dropped below 970 hpa. Using CFSR data, a budget of the primary terms of the EKE tendency equation was computed for each system using two slightly different methods. First, a box-integrated method was employed wherein the vertically-averaged components of baroclinic conversion were computed using the partitioned QG vertical velocity within quadrilaterals centered around the MSLP minimum of each cyclone with the hope of capturing the EKE tendency in the direct vicinity of each system. The divergence of ageostrophic geopotential fluxes were also computed within each quadrilateral, though the large geographical area covered by the boxes may have masked the amount of divergence in the direct vicinity of the surface cyclones. Second, these same budget terms were integrated within volumes defined by three EKE centers across the North Pacific in a manner similar to DGS in an attempt to document a potential case of downstream development as well as support results from the box-integrated method.

The three EKE centers consisted of 1) a “left” EKE center that was spatially tied to the developing western cyclone, 2) a “central” EKE center that developed between the western and eastern cyclones over the central North Pacific, and 3) a “right” EKE center that was associated with the developing eastern cyclone.

Results from the box-integrated method revealed that baroclinic conversion arising from shearwise vertical motions played a predominant role in the energetics evolution of each cyclone, albeit in different ways. The western cyclone was characterized by positive baroclinic conversion throughout its evolution, with shearwise baroclinic conversion outweighing transverse baroclinic conversion at the majority of the times analyzed. On the other hand, the eastern cyclone experienced negative baroclinic conversion during the early stages of its development. This negative conversion was driven by the shearwise component of vertical motions, whereas the transverse component of baroclinic conversion remained positive throughout the analysis period. Thus, until 00Z 7 October, the baroclinic conversion term served as a net sink of EKE for the eastern cyclone despite the fact that the system continued to strengthen during that time period. This growth was likely fostered by the convergence of ageostrophic geopotential fluxes emanating from both the western cyclone and an area of positive baroclinic conversion just upstream of the eastern cyclone. Indeed, the western cyclone exhibited a net divergence of ageostrophic geopotential fluxes throughout its evolution, although the box-integrated results indicated that the eastern cyclone experienced a net divergence of fluxes as well.

Results from the volume integrals supported the conclusion that the eastern cyclone received upstream energy to help foster its development. Energy dispersed by the left EKE center associated with the western cyclone contributed to the growth of a central EKE center further to the east. In turn, this central EKE center dispersed its own energy downstream to help develop the right EKE center associated with the eastern cyclone. As a result, the development of the eastern cyclone broadly follows the criteria listed by DGS and therefore qualifies as a case of downstream development. Furthermore, the volume-integrated results showed that the shearwise component of baroclinic conversion was dominant in the evolution of the overall baroclinic conversion for both the left and right EKE centers, supporting the results of the box-integrated method.

Thus, the preceding analysis revealed that shearwise vertical motions may contribute to a significant portion of the baroclinic conversion process, despite the fact that transverse vertical motions are, by definition, orientated to the baroclinicity in a much more favorable way for baroclinic conversion. In an attempt to explain this seemingly counterintuitive result, vertical cross-sections associated with each cyclone were examined in the hopes of obtaining information about potential differences in the vertical structure between the shearwise and transverse components of baroclinic conversion. The results of these cross-sections revealed that the shearwise baroclinic conversion was likely predominant because the shearwise vertical motions were more vertically in-phase with the maximum temperature anomalies than the transverse vertical motions. Furthermore, it was found that the shearwise baroclinic conversion tended to be concentrated in the middle and upper troposphere, whereas the transverse baroclinic conversion was more concentrated in the lower troposphere.

This suggested that the majority of baroclinic conversion was being performed in the middle and upper troposphere in association with the locations of the strongest shearwise vertical motions and temperature anomalies. To confirm this conjecture, a recalculation of the baroclinic conversion term was performed within three vertically partitioned layers throughout the atmospheric column, denoting contributions to the total baroclinic conversion from the 1) lower troposphere, 2) middle and upper troposphere, and 3) upper troposphere and lower stratosphere. It was found that the majority of the total baroclinic conversion was occurring in the middle and upper portions of the troposphere, with the shearwise component of baroclinic conversion predominating in these layers. The transverse component of baroclinic conversion tended to dominate in the lower troposphere and contributed much less overall to the total atmospheric column baroclinic conversion.

### b. Further Questions to Explore

The somewhat counterintuitive result that shearwise vertical motions were predominant in the baroclinic conversion process of the two extra-tropical cyclones examined in this study prompts further questions to explore in future work. Perhaps the most natural follow-up study would examine how common this result is in the context of developing extra-tropical cyclones. Either a climatology of recent cyclogenetic events or utilization of a real-time diagnostic tool to examine other cases would provide a larger sample size for a comparison of the prevalence of shearwise or transverse vertical motions as they relate to the baroclinic conversion process. Moreover, it is fair to wonder whether these results depend on the geographical region in question. Perhaps in locations where other EKE budget terms are more important, such as with the Reynolds stress term over North America (Lackmann et. al 1999), a different species of vertical motion may be predominant in the baroclinic conversion process as opposed to cases over oceanic basins. In addition, it may be worth examining whether changing the criteria for determining the perturbation temperature and wind fields could yield different outcomes. Calculating anomalies over a shorter time-scale may result in a different distribution of perturbation temperatures, possibly affecting the magnitude of the baroclinic conversion occurring in association with each cyclone.

Regardless of whether shearwise or transverse vertical motions are predominant within a specific cyclogenesis event, it would also be useful to examine the physical mechanisms driving the vertical motions in each case. For example, results from this study showed that shearwise vertical motions occurring in the middle and upper troposphere were responsible for the overall dominance of shearwise baroclinic conversion, which suggests that forcing mechanisms occurring in the upper troposphere may be the most important in driving the baroclinic conversion process. This would be consistent with results from Martin (2006) that showed shearwise motions in the middle and upper troposphere were predominant in the general cyclogenetic process. Since these shearwise vertical motions are a function of vorticity advection by the thermal wind (which is predominately a middle and upper tropospheric process), it may be the case that this forcing mechanism for vertical motion is integral to baroclinic conversion. If cases are found where transverse vertical motions are more predominant in driving baroclinic conversion, it would be useful to examine whether another forcing mechanism is instrumental in driving the vertical motions as part of the baroclinic conversion process. Perhaps deeper understanding of the EKE generation characteristics of extra-tropical cyclones will foster utility with regards to operational forecasting. Specifically, examination of forecast busts might reveal that more knowledge of the energetics evolution of prior synoptic disturbances could have led to better predictability of sensible weather events. For example, if a mid-latitude cyclone developed into a much stronger system than was previously forecast, an analysis of the energetics development associated with the system may provide an explanation as to why the cyclone grew stronger than originally anticipated. Any potential insights gleaned from such an analysis could then be applied to predictions of future cyclone developments to improve operational forecasting techniques.

# References

Danielson, R. E., J. R. Gyakum, and D. Straub, 2004: Examples of downstream baroclinic development among 41 cold-season eastern North Pacific cyclones. *Atmos.-Ocean*, **42**, 235-250.

Danielson, R. E., J. R. Gyakum, and D. Straub, 2006: A case study of downstream baroclinic development over the North Pacific Ocean. Part 1: Dynamical impacts. *Mon. Wea. Rev.*, **134**, 1534-1548.

Dare, P. M., and P. J. Smith, 1984: A comparison of observed and model energy balance for an extratropical cyclone system. *Mon. Wea. Rev.*, **112**, 1289-1308.

Davis, C. A., and K. A. Emanuel, 1991: Potential vorticity diagnostics of cyclogenesis. *Mon. Wea. Rev.*, **119**, 1929-1953.

Eliassen, A., 1962: On the vertical circulation in frontal zones. *Geofys. Publ.*, **24**, 147-160.

Hoskins, B. J., I. Draghici, and H. C. Davies, 1978: A new look at the omega equation. *Quart J. Roy. Meteor. Soc.*, **104**, 31-38.

Hoskins, B. J., M. E. McIntyre, and A. W. Robertson, 1985: On the use and significance of isentropic potential vorticity maps. *Quart. J. Roy. Meteor. Soc.*, **111**, 877-946.

Keyser, D., B. D. Schmidt, and D. G. Duffy, 1992: Quasigeostrophic vertical motions diagnosed from along- and cross-isentrope components of the Q vector. *Mon. Wea. Rev.*, **120**, 731-741.

Kung, E. C., 1977: Energy sources in middle-latitude synoptic-scale disturbances. *J. Atmos. Sci.*, **34**, 1352-1365.

Kutzbach, G., 1979: The thermal theory of cyclones. *Quart. J. Roy. Meteor. Soc.*, **106**, 625–626.

Lackmann, G. M., D. Keyser, and L.F. Bosart, 1997: A characteristic life cycle of upper-tropospheric cyclogenetic precursors during the Experiment on Rapidly Intensifying Cyclones over the Atlantic (ERICA). *Mon. Wea. Rev.*, **125**, 2729-2758.

Lackmann, G. M., D. Keyser, and L.F. Bosart, 1999: Energetics of an intensifying jet streak during the Experiment on Rapidly Intensifying Cyclones over the Atlantic (ERICA). *Mon. Wea. Rev.*, **127**, 2777-2795.

Lang, A. A., and J. E. Martin, 2010: The influence of rotational frontogenesis and its associated shearwise vertical motions on the development of an upper-level front. *Quart. J. Roy. Meteor. Soc.*, **136**, 239-252.

Lang, A. A., and J. E. Martin, 2012: The structure and evolution of lower stratospheric frontal zones. Part I: Examples in northwesterly and southwesterly flow. *Quart. J. Roy. Meteor. Soc.*,**138**, 1350-1365.

Lang, A. A., and J. E. Martin, 2013b: The structure and evolution of lower stratospheric frontal zones. Part II: The influence of tropospheric convection on lower stratospheric frontal development. *Quart. J. Roy. Meteor. Soc.*, **139**, 1798-1809.

Martin, J. E., 1998a: The structure and evolution of a continental winter cyclone. Part I: Frontal structure and the classical occlusion process. *Mon. Wea. Rev.*, **126**, 303-328.

Martin, J. E., 1998b: The structure and evolution of a continental winter cyclone. Part II: Frontal forcing of an extreme snow event. *Mon. Wea. Rev.*, **126**, 329-347.

Martin, J. E., 1999a: Quasi-geostrophic forcing of ascent in the occluded sector of cyclones and the trowal airstream. *Mon. Wea. Rev.*, **127**, 70-88.

Martin, J. E., R. A. Grauman, and N. Marsili, 2001: Surface cyclolysis in the north Pacific Ocean. Part 1: A synoptic-climatology. *Mon. Wea. Rev.*, **129**, 748-765.

Martin, J. E., 2006: The role of shearwise and transverse quasi-geostrophic vertical motions in the mid-latitude cyclone life cycle. *Mon. Wea. Rev.,***134**, 1174-1193.

Martin, J. E., 2007: Lower-tropospheric height tendencies associated with the shearwise and transverse components of quasi-geostrophic vertical motion. *Mon. Wea. Rev.*, **135**, 2803-2809.

Martin, J. E., 2014: Quasi-gesotrophic diagnosis of the influence of vorticity advection on the development of upper level jet-front systems. *Quart. J. Roy. Meteor. Soc.*, **140**, 2658-2671.

McLay, J. G., and J. E. Martin, 2002: Surface cyclolysis in the north Pacific Ocean. Part III: Composite local energetics of tropospheric-deep cyclone decay associated with rapid surface cyclolysis. *Mon. Wea. Rev.*, **130**, 2507-2529.

Namias, J., and P. F. Clapp, 1944: Studies of the motion and development of long waves in the westerlies. *J. Meteor.*, **1**, 57-77.

Orlanski, I., and J. Katzfey, 1991: The life cycle of a cyclone wave in the Southern Hemisphere. Part 1: Eddy energy budget. *J. Atmos. Sci.*, **48**, 1972-1998.

Orlanski, I., and J. P. Sheldon, 1993: A case of downstream baroclinic development over western North America. *Mon. Wea. Rev.*, **121**, 2929-2950.

Orlanski, I., and J. P. Sheldon, 1995: Stages in the energetics of baroclinic systems. *Tellus*, **47A**, 605-628.

Papritz, L., and S. Schemm, 2013: Development of an idealised downstream cyclone: Eulerian and Lagrangian perspective on the kinetic energy. *Tellus A*, **65**, 19539, http://dx.doi.org/10.3402/tellusa.v65i0.19539.

Pettersen, S., 1956: *Weather Analysis and Forecasting,* Volume 1: *Motion and motion systems.* McGraw Hill, 428 pp.

Robertson, F. R., and P. J. Smith, 1983: The impact of model moist processes on the energetics of extratropical cyclones. *Mon. Wea. Rev.*, **111**, 723-744.

Roebber, P. J., 1984: Statistical analysis and updated climatology of explosive cyclones. *Mon. Wea. Rev.*, **112**, 1577-1589.

Sanders, F., and J. R. Gyakum, 1980: Synoptic-dynamic climatology of the “Bomb”. *Mon. Wea. Rev.*, **108**, 1589-1606.

Sawyer, J. S., 1956: The vertical circulation at meteorological fronts and its relation to frontogenesis. *Proc. Roy. Soc. London*, **A234**, 346-362.

Schemm, S., H. Wernli, and L. Papritz, 2013: Warm conveyor belts in idealized moist baroclinic wave simulations. *J. Atmos. Sci.*, **70**, 627-652.

Shapiro, M. A., 1981: Frontogenesis and geostrophically forced secondary circulations in the vicinity of jet stream-frontal zone systems. *J. Atmos. Sci.*, **38**, 954-973.

Sutcliffe, R. C., 1947: A contribution to the problem of development. *Quart. J. Roy. Meteor. Soc.*, **73**, 370-383.

Trenberth, K. E., 1978: On the interpretation of the diagnostic quasi-geostrophic omega equation. *Mon. Wea. Rev.*, **106**, 131-137.

Winn-Nielsen, A., 1959: On the application of trajectory methods in numerical forecasting. *Tellus*, **11**, 180-196.